Published in final edited form as:
Nat Genet. 2021 March 01; 53(3): 392–402. doi:10.1038/s41588-020-00776-w.

Genome-wide meta-analysis, fine-mapping, and integrative prioritization implicate new Alzheimer's disease risk genes

Jeremy Schwartzentruber[1,2,3,*], **Sarah Cooper**[2,3], **Jimmy Z. Liu**[4], **Inigo Barrio-Hernandez**[1,2], **Erica Bello**[2,3], **Natsuhiko Kumasaka**[3], **Adam M. H. Young**[5], **Robin J. M. Franklin**[5], **Toby Johnson**[6], **Karol Estrada**[7], **Daniel J. Gaffney**[2,3,8], **Pedro Beltrao**[1,2], **Andrew Bassett**[2,3,*]

[1]European Molecular Biology Laboratory, European Bioinformatics Institute (EMBL-EBI), Wellcome Genome Campus, Cambridge, UK

[2]Open Targets, Wellcome Genome Campus, Cambridge, UK

[3]Wellcome Sanger Institute, Wellcome Genome Campus, Cambridge, UK

[4]Biogen, Cambridge, MA, USA

[5]Wellcome-Medical Research Council Cambridge Stem Cell Institute, Cambridge Biomedical Campus, University of Cambridge, Cambridge, UK

[6]Target Sciences-R&D, GSK Medicines Research Centre, Stevenage, UK

[7]BioMarin Pharmaceutical, San Rafael, CA, USA

[8]Genomics Plc, Oxford, UK

Abstract

Genome-wide association studies (GWAS) have discovered numerous genomic loci associated with Alzheimer's disease (AD), yet the causal genes and variants remain incompletely identified. We performed an updated genome-wide AD meta-analysis, which identified 37 risk loci, including novel associations near *CCDC6*, *TSPAN14*, *NCK2*, and *SPRED2*. Using three SNP-level fine-mapping methods, we identified 21 SNPs with greater than 50% probability each of being causally involved in AD risk, and others strongly suggested by functional annotation. We followed this with colocalization analyses across 109 gene expression quantitative trait loci (eQTL) datasets, and prioritization of genes using protein interaction networks and tissue-specific expression. Combining this information into a quantitative score, we find that evidence converges on likely

*Jeremy Schwartzentruber (jeremys@ebi.ac.uk), Andrew Bassett (ab42@sanger.ac.uk).

Author Contributions

J.S. planned and conducted the analyses, and wrote the paper. J.Z.L. performed the GWAX and meta-analysis. S.C. and E.B. assisted with fine-mapping, variant and gene prioritization. I.B.-H. and P.B. performed and supervised gene network analysis. R.J.M.F. designed and A.M.H.Y. performed the isolation of human microglia from brain biopsies. N.K. performed microglia eQTL mapping. A.B., T.J., D.J.G., and K.E. conceived and supervised the study.

Competing interests

J.Z.L. was an employee of Biogen at the time of the study, and is now an employee of GSK. D.J.G. is an employee of Genomics Plc. T.J. is an employee of GSK. K.E. is an employee of BioMarin Pharmaceutical.

Europe PMC Funders Author Manuscripts

causal genes, including the above four genes, and those at previously discovered AD loci, including *BIN1*, *APH1B*, *PTK2B*, *PILRA*, and *CASS4*.

Genome-wide association studies (GWAS) for family history of disease, known as GWAS-by-proxy (GWAX), are a powerful method for performing genetic discovery in large, unselected cohort biobanks, particularly for age-related diseases[1]. Recent meta-analyses have combined GWAS of diagnosed late-onset Alzheimer's disease (AD) with GWAX for family history of AD in the UK Biobank[2,3], and reported 12 novel disease-associated genomic loci. However, the causal genetic variants and genes which influence AD risk at these and previously discovered loci have only been clearly identified in a few cases. Discovering causal variants has led to deeper insight into molecular mechanisms of multiple diseases, including obesity[4], schizophrenia[5], and inflammatory bowel disease[6]. For AD, known causal variants include the $\varepsilon 4$ haplotype in *APOE*, the strongest genetic risk factor for late-onset AD, and a common nonsynonymous variant that strongly alters splicing of *CD33* exon 2[7]. Likely causal rare nonsynonymous variants have also been discovered in *TREM2*[8], *PLCG2* and *ABI3*[9]. These findings have strengthened support for a causal role of microglial activation in AD.

Although non-synonymous variants are highly enriched in trait associations, most human trait-associated variants do not alter protein-coding sequence and are thought to mediate their effects via altered gene expression, which is likely to occur in a cell type-dependent manner. A growing number of studies have mapped genetic variants affecting gene expression, known as expression quantitative trait loci (eQTLs), in diverse tissues or sorted cell types[10,11]. While it has become common to integrate GWAS results with eQTLs, this is often limited to a small number of datasets thought to be relevant.

To identify putative causal genetic variants for AD, we performed a meta-analysis of GWAX in the UK Biobank with the latest GWAS for diagnosed AD[12], followed by fine-mapping using three alternative methods. Notably, this updated GWAS tested more genetic variants than the Lambert et al. study[13] used in meta-analyses by Jansen et al.[3] and Marioni et al.[2] (11.5 vs. 7.1 million). The increased power from our meta-analysis revealed four additional AD risk loci, and the higher density genotype imputation identified new candidate causal variants at both novel and established loci. We also performed statistical colocalization analyses with a broad collection of eQTL datasets, including a recent study on primary microglia[14], to identify candidate genes mediating risk at AD loci. We find that multiple lines of evidence, including colocalization, tissue- or cell type-specific expression, and information propagation in gene networks, converge on a set of likely causal AD genes.

Results

Meta-analysis discovers 37 loci associated with Alzheimer's disease risk

We performed a GWAX in the UK Biobank for family history of AD, based on 53,042 unique individuals who were either diagnosed with AD or who reported a parent or sibling having dementia, and 355,900 controls. This identified 13 risk loci ($P < 5 \times 10^{-8}$), 10 of which have been reported previously. Three novel loci were located near *NCK2*, *PRL*, and

Europe PMC Funders Author Manuscripts

FAM135B. Notably, *PRL* has been reported as a CSF biomarker of AD[15]. We next did a fixed-effects meta-analysis of these GWAX results with the Kunkle et al. stage 1 GWAS meta-analysis of 21,982 cases with diagnosed AD and 41,944 controls[12], across 10,687,126 overlapping variants (Fig. 1). This revealed 34 AD risk loci ($P < 5 \times 10^{-8}$), 22 of which were reported in Kunkle et al., while 8 others were reported in either Jansen et al.[3] or Marioni et al.[2]. Four loci were novel, located near *NCK2*, *TSPAN14*, *SPRED2*, and *CCDC6*. Notably, the *PRL* and *FAM135B* regions showed no evidence of association in Kunkle et al. ($P > 0.1$), and hence were not significant in meta-analysis. We included 37 loci in our follow-up analyses, which included three loci found at suggestive significance ($P < 5 \times 10^{-7}$) near *IKZF1*, *TSPOAP1*, and *TMEM163* (Fig. 1 and Supplementary Table 1). LD score regression[16] showed that most of the inflation in summary statistics was due to the polygenicity of AD rather than confounding by population structure (lambda_GC = 1.140, intercept = 1.0285 with SE = 0.0069; Supplementary Table 2). Of our 37 loci, 16 were nominally replicated ($P < 0.05$) in either the Gr@ace study[17] (4,120 probable AD cases and 3,289 controls) or the FinnGen biobank (v3, 3,697 cases and 131,941 controls) (Supplementary Table 3). Among our four novel loci, only *TSPAN14* replicated with $P < 0.05$ (in FinnGen), although power was limited in these smaller datasets (estimated at 28-76%), and most of the alleles had concordant directions of effect. In a meta-analysis with all four datasets, support for most loci was strengthened (Extended Data Fig. 1), including novel loci *TSPAN14*, *CCDC6* and *NCK2*, but was weakened for *SPRED2* (meta-analysis $P = 1.3 \times 10^{-7}$). Although not included in downstream analyses, four new loci became genome-wide significant, near *GRN*, *IGHG1*, *SHARPIN*, and *SIGLEC11* (Supplementary Table 3).

Next, we applied stepwise conditioning using GCTA[18], with linkage disequilibrium (LD) determined from UK Biobank samples, to identify independent signals at the discovered loci. Apart from *APOE*, 9 loci had two independent signals, while the *TREM2* locus had three signals (Fig. 1c). Interestingly, a number of the loci discovered recently[2,3,12] had multiple signals: *NCK2*, *EPHA1*, *ADAM10*, *ACE*, and *APP-ADAMTS1*. To extract insight from both new and established AD GWAS discoveries, we performed comprehensive colocalization, annotation, fine-mapping and network analyses to identify causal genes and variants (Fig. 1a).

Colocalization between AD risk loci and gene expression traits

To identify genes whose expression may be altered by risk variants, we performed statistical colocalization[19] between each of 36 risk loci (excluding *APOE*) and a set of 109 eQTL datasets representing a wide variety of tissues, cell types and conditions (Fig. 2 and Supplementary Table 4). The eQTL datasets include a study of primary microglia from 93 brain surgery donors[14], a meta-analysis of 1,433 brain cortex samples[20], 49 tissues from GTEx[11], and 57 eQTL datasets uniformly reprocessed as part of the eQTL catalogue[10]. The latter include multiple studies in tissues of potential relevance to AD, such as brain, as well as sorted blood immune cell types under different stimulation conditions[21–37]. For each gene, the colocalization analysis reports the probability that the GWAS and eQTL share a causal variant, referred to as hypothesis 4 (H4).

Europe PMC Funders Author Manuscripts

Some studies using colocalization have suggested that there is relatively limited overlap between GWAS associations and eQTLs above that expected by chance[6,38]. A possible reason is that colocalization analyses can have low sensitivity to detect shared causal variants between traits, which could occur for a number of reasons. First, when a locus has multiple causal variants, and not all causal effects are shared between the two studies, colocalization may not be detected[19]. Second, if the relevant tissue, cell type, or cellular context has not been assayed, then a colocalization may not be found. Third, differences in LD patterns between studies can reduce the likelihood of a positive colocalization. Lastly, low power in either study can further reduce the colocalization probability. To mitigate the first effect, we performed colocalizations separately for each conditionally independent AD signal, to model the case where not all causal variants are shared, as well as for the combined AD signal at each locus. Problems relating to power, LD mismatch, or missing the relevant cell type or context are partially mitigated by our use of a large number of highly-powered eQTL datasets, which include those with stimulated conditions.

Across the 36 loci, we found 391 colocalizations with at least 80% probability of a shared causal variant between AD and eQTL, representing 80 distinct genes at 27 loci (Supplementary Tables 5 and 6). The genes implicated by colocalization include many that have previously been investigated for roles in AD, such as *PTK2B* [39,40], *BIN1* [41,42], *PILRA* [43], *CD33* [44,45], and *TREM2* [46,47], as well as novel candidates including *FCER1G*, *TSPAN14*, *APH1B*, and *ACE*. However, the presence of multiple genes with colocalization evidence within individual loci suggests that additional lines of evidence are important for prioritizing relevant genes.

Fine-mapping identifies credibly causal variants

Confirming the causal genes underlying AD risk will ultimately require experiments to identify the molecular mechanisms by which gene function is altered. Such experiments must be motivated by strong hypotheses regarding potentially causal variants and their possible effects. To identify candidate causal variants, we used three distinct fine-mapping methods: single causal variant fine-mapping[48] on each conditionally independent signal; FINEMAP[49], limiting the number of causal variants at each locus to the number of signals determined by GCTA; and PAINTOR[50], a method that leverages enrichments in functional genomic annotations to improve causal variant identification (see Methods).

As a reference panel for our analyses, we used LD computed from UK Biobank participants. Previous work has shown that using reference panels that are either too small or poorly matched can result in spurious fine-mapping signals[51]. For this reason, we conducted a sensitivity analysis (described in the Supplementary Note) by using the same reference panel for conditional analysis and fine-mapping on the non-UK Biobank portion of our meta-analysis (Kunkle et al.). This gave comparable independent signals and SNP probabilities to the full meta-analysis, with the exception of a few loci, namely *ABCA7*, *HLA*, *EPHA1*, and *ECHDC3* (Extended Data Fig. 2).

We used 44 annotations individually as input to PAINTOR (Supplementary Table 7); these included ATAC-seq peaks from primary microglia[52] or iPSC-derived macrophages[53], DNase peaks from the Roadmap Epigenomics project[54], variant consequence annotations[55], and

evolutionary conservation[56] (Fig. 3). We also used scores from DeepSEA[57] and SpliceAI[58], deep-learning methods that predict the effects of variants on transcription factor binding or splicing. Missense mutations were the most enriched annotation, with 19.2-fold increased odds of being causal SNPs, but they comprised only 1% of input SNPs. Blood or immune DNase hypersensitivity peaks merged from 24 Roadmap Epigenomics tissues provided the highest model likelihood, as these peaks covered 16% of SNPs, despite a lower 6.4-fold enrichment. Variants with a non-zero score from SpliceAI, which predicts changes to gene splicing, were also highly enriched (9.3-fold).

We next built a multi-annotation model in PAINTOR following a stepwise selection procedure, which identified a minimal but informative set of three annotations: blood and immune DNase, nonsynonymous coding variants, and variants with SpliceAI score greater than 0.01. We used probabilities from this PAINTOR model, and computed the mean causal probability per variant across the three fine-mapping methods.

There were 21 variants with mean causal probability above 50% across the fine-mapping methods, and 79 further variants with probabilities from 10-50% (Table 1 and Supplementary Table 8). These include SNPs near established AD risk genes, such as rs6733839 ~20 kb upstream of *BIN1*, which has recently been shown to alter a microglial MEF2C binding site[14] and to regulate *BIN1* expression specifically in microglia[42]. High-confidence variants also include a well-known missense SNP in *PILRA* [43], and a splice-altering missense SNP in *CD33* [7]. Missense SNP rs4147918 in *ABCA7* had 55% causal probability, and *ABCA7* harbored 5 further missense SNPs with probabilities greater than 0.01%, at varying allele frequencies. Notably, rs4147918 and 6 other variants within *ABCA7*, including the lead SNP rs12151021, had positive SpliceAI scores. This is consistent with reports of a burden of deleterious variants at *ABCA7* associated with AD[59], as well as potential changes to splicing caused by intronic variable tandem repeats[60].

A number of newly identified AD risk genes had high-confidence fine-mapped variants. These include the *NCK2* rare intronic SNP rs143080277 (>99% probability, MAF 0.4%), *APH1B* missense SNP rs117618017 (90% probability), rs2830489 near *ADAMTS1* (72% probability), and rs268120 intronic in *SPRED2* (56% probability).

Manual review highlighted a number of candidate causal variants, where the annotation-based SNP probability was higher than that of the other two methods (Fig. 4). Within *TSPAN14*, rs1870137 and rs1870138 reside within a DNase hypersensitivity peak found broadly across tissues, which is also an ATAC peak in microglia. Of these, rs1870138 lies at the centre of a ChIP-seq peak for binding of multiple transcription factors, including FOS/JUN and GATA1. The AD risk allele rs1870138-G alters an invariant position of a binding motif for *TAL1*, a gene highly expressed in microglia, and which is a binding partner for GATA1. This allele is also associated with increased monocyte count[71] and increased risk for inflammatory bowel disease[72]. Notably, the AD signal in the region colocalizes with both an eQTL and a splicing QTL for *TSPAN14* in multiple datasets, and rs1870138-G associates with higher *TSPAN14* expression in brain and in microglia, but with lower expression in some GTEx tissues.

Missense SNP rs117618017 in exon 1 of *APH1B* (Thr27Ile) is the likely single causal variant at its locus, with fine-mapping probability of 90% (Fig. 4b). APH1B is a component of the gamma-secretase complex, other members of which (*PSEN1*, *PSEN2*) have rare variants associated with early-onset AD[73]. Interestingly, the AD signal colocalizes with an *APH1B* eQTL in monocytes, neutrophils and T-cells, and rs117618017-T associates with higher AD risk and higher *APH1B* expression across datasets. This allele introduces a motif for transcriptional regulator YY1, and is predicted by DeepSEA to increase YY1 binding in multiple ENCODE cell lines. Therefore, it is an open question whether AD risk is mediated by altered APH1B protein structure or altered gene expression.

Finally, the AD association on chromosome 20 colocalizes with an eQTL for *CASS4* in Blueprint monocytes and in GTEx whole blood. While intronic lead SNP rs6014724 (55% probability) shows no evidence of transcription factor (TF) binding in ENCODE data, rs17462136 (7% probability) lies in a region of dense TF binding in the 5' UTR of *CASS4* (Fig. 4c). The nucleotide position is highly conserved (GERP score 3.46) and overlaps an ATAC peak in microglia, and the rs17462136-C allele introduces a TEAD1 binding motif. In addition, rs17462136 is more strongly associated with *CASS4* expression in multiple eQTL datasets than is rs6014724.

Network evidence prioritizes genes within and beyond GWAS loci

As a further line of evidence, we developed a method that leverages gene network connectivity to prioritize genes at individual loci. We first constructed a gene interaction network combining information from the STRING, IntAct and BioGRID databases. Next, we nominated 32 candidate AD genes (Supplementary Table 9), based on our other evidence sources as well as literature reports, and used these as seed genes similar to the approach used in the priority index for drug discovery[74]. For each locus in turn, we used as input all seed genes except those at the locus, and propagated information through the network with the page rank algorithm. The "networkScore" for a gene thus represents the degree to which the gene is supported by its interaction with top AD candidate genes at other loci, unbiased by any locus-specific features.

Across AD loci, our selected seed genes were highly enriched for having high network-based gene scores (one-tailed Wilcoxon rank sum test, $P = 5 \times 10^{-9}$; Extended Data Fig. 3). At our four novel AD loci, the nearest gene (*NCK2*, *TSPAN14*, *SPRED2*, *CCDC6*) in each case was one of the top two highest-scoring genes within 500 kb. Many established or recently discovered AD genes were also the top gene within 500 kb by network score, including *ACE*, *BIN1*, *CASS4*, *CD2AP*, *PICALM*, *PLCG2*, and *PTK2B*. At the *SLC24A4* locus, *RIN3* was strongly supported, whereas *SLC24A4* was not, in line with evidence from deleterious rare variants that *RIN3* may be causal[12].

Genes highly ranked by network propagation also include many outside of genome-wide significant AD loci (Supplementary Table 10). Consistent with their involvement in AD, such genes tended to have SNPs with lower *P* values nearby than did remaining genes (Fig. 5a and Extended Data Fig. 3c), suggesting that numerous AD loci remain to be discovered with larger GWAS sample sizes. Top network-ranked genes include *LILRB2* (nearby rs3855678 $P = 9.8 \times 10^{-6}$), which encodes a leukocyte immunoglobulin-like receptor that

recognizes multiple HLA alleles, and which may also be involved in amyloid-beta fibril growth[75]; *ABCA1* (rs59237458 $P = 4 \times 10^{-6}$), involved in phospholipid transfer to apolipoproteins and previously associated with AD[76]; *SREBF1* (rs35763683 $P = 2 \times 10^{-6}$), required for lipid homeostasis; and *AGRN* (rs2710871 $P = 4 \times 10^{-6}$), involved in synapse formation in mature hippocampal neurons. Overall, genes with high network ranks were strongly enriched in biological processes and pathways that have previously been associated with AD, including clathrin-mediated endocytosis, activation of immune response, phagocytosis, Ephrin signaling, and complement activation (Supplementary Table 11).

AD risk is enriched near genes with high microglial gene expression

To understand the contribution of cell-type specific gene expression to AD risk, we used fgwas[78] to assess the genome-wide enrichment of SNPs near genes highly expressed in specific cell types, based on a single-nucleus sequencing dataset of 49,495 nuclei from six human brain cortical areas[77,79]. Out of 18 broad cell type clusters, only microglia showed clear enrichment of AD risk (odds ratio (OR) 6.0) near genes with expression above the 90th percentile across cell types (Fig. 5b). We performed a similar analysis looking at bulk gene expression across human tissues from GTEx, along with a small number of additional RNA-seq datasets, including sorted primary microglia from brain surgeries[14] (Extended Data Fig. 4 and Supplementary Table 12). This gave consistent results, with microglia showing strong enrichment (OR 4.4), followed by tissues rich in immune cells, including spleen (OR 3.6) and whole blood (OR 3.2). Notably, iPSC-derived microglia showed similar enrichment to primary microglia, while bulk brain tissues (including hippocampus) showed no enrichment.

Integrative gene prioritization from five lines of evidence

Determining the genes responsible for AD risk across GWAS loci is challenging, in part because few genes have been definitively confirmed as having a causal role. We therefore developed a comprehensive gene prioritization score, which incorporates quantitative information based on five lines of evidence: gene distance to lead SNPs, colocalization, network score, bulk and single-cell gene expression, and the sum of fine-mapped probability for any coding SNPs within a gene (Fig. 6, Extended Data Figs. 5 and 6, and Supplementary Table 13).

We first explored how best to use colocalization information. We found that genes with maximum colocalization probability (maxH4) above 0.9 had higher prioritization scores based on the other four predictors, but this was not the case for genes with weaker colocalization evidence (Extended Data Fig. 5a). We also examined colocalizations in different cell type or tissue groups, such as brain, microglia, and other GTEx tissues. There was little evidence that colocalizing genes within any specific groups had higher total scores than other groups (Extended Data Fig. 5b), although this conclusion was limited by the low number of studies in some cell types, such as microglia. We therefore based our colocalization score on the maximum colocalization probability across tissues (> 0.9) and normalized this to the range 0-1.

A priori, we do not know which lines of evidence are most important for prioritizing genes. We therefore sought a systematic way to identify appropriate weights for the predictors.

Europe PMC Funders Author Manuscripts

Although we do not know the causal AD genes, we selected two independent, unbiased sets of candidate genes for use in supervised learning: genes nearest to the GWAS peaks, and genes with high network scores (>80th percentile). In order to identify weights for our predictive features, we defined two models to discriminate these two gene sets from others within 500 kb, in each case using cross-validated lasso-regularized logistic regression with the remaining variables as predictors. As expected, when predicting genes nearest GWAS peaks, the highest-weight predictor was fine-mapped coding variants; however, only a few loci have such variants. The most informative predictor, determined based on change in mean-squared error when the predictor is left out, was colocalization, followed by coding variants and then network score (Supplementary Table 14). When predicting high network score genes, the most informative predictor was distance to GWAS peak, followed by microglial gene expression, and neither colocalization nor coding variant predictors improved the model. For both models, including hippocampus expression (GTEx) or single-cell astrocyte expression resulted in worse models (increased mean squared error).

We defined our gene prioritization “model score” as the average of the predictions from our two models. The model score identified as top-ranked many AD candidate genes previously suggested as causal (Fig. 6). Exemplifying the importance of integrating genetic evidence sources, *ABCA7*, *SORL1*, and *CR1* were top-ranked by overall score at their respective loci, despite having only moderate network-based scores, while *SORL1, PICALM*, and *SPI1* were top-ranked despite having limited eQTL colocalization evidence.

While our prioritization further supports many established AD candidate genes, it also implicates novel genes. Among these are *FCER1G*, which has been reported as a hub gene in microglial gene modules associated with neurodegeneration[81,82], and has been experimentally shown to influence microglial phagocytosis[83]. Another candidate is *ZYX*, which receives a top network score, is highly expressed in microglia, and which was recently nominated as an AD risk gene based on chromatin interactions between the *ZYX* promoter and AD risk variants in a *ZYX* enhancer[84].

Discussion

Identifying therapeutic targets for human diseases is a key goal of human genetics research, and is particularly important for neurodegenerative diseases such as AD, for which no disease-modifying therapies yet exist. However, identifying the causal genes and genetic variants from GWAS is challenging, since non-coding associations can act via regulation of distal genes. We approached this challenge for AD by performing comprehensive fine-mapping, eQTL colocalization, network analysis, and quantitative gene prioritization.

Our meta-analysis identified four novel associations near *NCK2*, *SPRED2*, *TSPAN14*, and *CCDC6*. Each of these was the nearest gene to the association peak and was supported by both eQTL colocalization and network ranking. Yet, despite the large number of eQTL datasets that we used, colocalization of likely AD risk genes was sometimes found in only one or a few datasets; this was the case for *SPRED2* (TwinsUK LCL coloc probability 0.99), *RIN3* (GTEx frontal cortex probability 0.94), and *PILRA* (Fairfax LPS-2hr monocyte coloc probability 0.99). Many factors could account for dataset-specific colocalizations, such as

biological differences in sample state, differences in LD match between the GWAS and eQTL datasets, and technical differences in the transcriptome annotations used for eQTL discovery. As a result, absence of colocalization provides only weak evidence for lack of an effect in a given tissue type, whereas positive colocalization provides strong support for a shared genetic effect. It is therefore useful to look broadly across eQTL studies for colocalization, which will be facilitated by resources that simplify access to these datasets, such as the eQTL catalogue[11].

One of our most confidently prioritized genes was *APH1B*, encoding a gamma-secretase complex component involved in APP processing. *APH1B* harbors the likely causal missense variant T27I, yet also has strong colocalization evidence that higher expression correlates with higher AD risk. One possibility is that impaired function of *APH1B* due to the missense variant leads to upregulation of *APH1B* transcription. This interpretation would be consistent with evidence from both mice[86] and humans[87] that loss of APH1B and gamma-secretase function leads to AD. It is noteworthy, however, that recent experiments failed to find an effect of the T27I variant on gamma-secretase activity in HEK cells[88].

Among our novel associations, TSPAN14 has a role in defining the localization of ADAM10[90], another recently discovered AD gene that is a key component of the alpha-secretase complex and that could thus mediate AD risk via processing of amyloid precursor protein. However, ADAM10 also cleaves the microglia-associated protein TREM2 to generate its soluble ligand-binding domain[91]. Our fine-mapping showed that the risk SNP rs1870138 is also associated with higher risk for inflammatory bowel disease (IBD), an immune-mediated disease, and with higher monocyte count in UK Biobank participants. Since *TSPAN14* is expressed more highly in immune cell types, including microglia, than in brain tissue, it is also plausible that AD risk is mediated by its effect on either immune cell count or activation. Recently proposed AD candidate genes supported by our analyses include *RIN3*, *HS3ST1*, and *FCER1G*. As noted above, FCER1G is a microglial master regulator[81–83]; RIN3 interacts with both BIN1 and CD2AP in the early endocytic pathway[93]; HS3ST1 is involved in cellular uptake of tau[94] and was recently been associated with AD in an independent Norwegian sample[62].

In summary, our study reports quantitative gene prioritization for 36 AD-associated regions, as well as AD-specific gene network scores beyond these loci. Our genetic findings highlight the presence of diverse mechanisms in AD pathogenesis and suggest candidate targets for therapeutic development.

Online Methods

GWAS on family history of AD

Sample QC, variant QC and imputation was performed on all UK Biobank (UKB) participants as described in Bycroft et al.[95]. After genotype imputation, 93,095,623 variants across 487,409 individuals were available for analysis. To exclude individuals of non-European ancestry, we extracted “White British” ancestry participants as described in Bycroft et al.[95]. These individuals self-reported their ethnic background as “British” and have similar genetic ancestry based on principal components (PC) analysis. To extract

Europe PMC Funders Author Manuscripts

additional individuals of European ancestry, we followed a similar approach to Bycroft et al. and applied Aberrant[96] on PCs 1v2, 3v4 and 5v6 across the individuals who self-reported as "Irish" or "Any other white background". We identified first-degree relatives by applying KING[97] v2.0 to 147,522 UKB participants who had at least one relative identified in Bycroft et al. (UKB Field 22021). For each first-degree relative pair, we prioritized AD cases and proxy-cases (see below) for inclusion, and otherwise excluded one of the pair at random. We also excluded variants with low imputation quality (INFO < 0.3) and/or those with minor allele frequencies below 0.0005, resulting in 25,647,815 variants available for analysis.

AD cases were extracted from UKB self-report (field 20002), ICD10 diagnoses (fields 41202 and 41204) and ICD10 cause of death (fields 40001 and 40002) data. UKB participants were asked whether they have a biological father, mother or sibling who suffered from Alzheimer's disease/dementia (UKB fields 20107, 20110, and 20111, respectively). We extracted all participants with at least one affected relative as proxy-cases. Participants who answered "Do not know" or "Prefer not to answer" were excluded from analyses. All remaining individuals were denoted as controls.

There were 898 AD cases, 52,791 AD proxy cases and 355,900 controls in the combined white British and white non-British cohorts. For association analyses, we lumped the true and proxy-cases together (53,042 unique affected individuals) and used the linear-mixed model implemented in BOLT-LMM[98].

AD meta-analysis

To enable meta-analysis combining the UKB cohorts with external case-control studies, we first transformed the AD proxy BOLT-LMM summary statistics from the linear scale to a 1/0 log odds ratio:

$$logOR \approx \beta_{LMM}/(f(1-f))$$

with standard error:

$$se \approx se_{LMM}/(f(1-f))$$

where β_{LMM} and se_{LMM} are the SNP effect sizes and standard errors respectively from BOLT-LMM, and f is the fraction of cases in the sample[99]. Since the affected individuals in our analysis include both true and proxy-cases, we then multiplied the transformed logORs and standard errors by 1.897 to approximate the logORs obtained from a true case/control study[1].

We combined the transformed UKB white British cohort, UKB white non-British cohort and the Stage 1 summary statistics from Kunkle et al. using a fixed-effects (inverse variance weighted) meta-analysis across 10,687,126 overlapping variants. For display purposes (Supplementary Table 8), we used CrossMap[100] to convert variant positions from GRCh37 to GRCh38.

Replication

To assess replication of our discovered signals, we downloaded the publicly available summary statistics for the Gr@ace study of AD[17] from the GWAS catalog, and for the FinnGen GWAS of phenotypes “Alzheimer’s disease, wide definition” and “Alzheimer’s disease (Late onset)” from FinnGen release 3. We extracted summary results for our lead SNPs, or a partner in strong LD when the lead SNP was not found, and present these in Supplementary Table 3. We estimated power to detect our four novel loci at nominal significance ($P < 0.05$) using the genetic power calculator (zzz.bwh.harvard.edu/gpc/cc2.html) with the genotype relative risks estimated from our meta-analysis, and the allele frequency and case/control count from the GWAS study of interest (Gr@ace or FinnGen), and assuming a disease prevalence of 5%. We performed an inverse variance-weighted meta-analysis of all four studies (Kunkle et al., UKB, Gr@ace, and FinnGen “AD wide”), similar to our discovery meta-analysis.

Conditional analysis and statistical fine-mapping

To run GCTA, we prepared plink input files with genotypes from 10,000 randomly sampled UKB individuals at variants within +/- 5 Mb from each lead SNP. We excluded variants with INFO < 0.85, or which had a *P*-value from Cochran’s Q test for study heterogeneity < 0.001. We also excluded variants with minor allele frequency (MAF) in UKB below 0.1%, as LD estimates are unreliable at low allele counts. We selected these thresholds after manual examination of fine-mapping results, where we found that more lenient cutoffs led either FINEMAP or PAINTOR to select implausible causal variants at a few loci, such as pairs of very weakly associated rare variants to explain a common variant signal. We ran GCTA (v1.92.1) --cojo-slct with a threshold of $P < 10^{-5}$ to identify secondary signals at each locus, and then retained only loci with a lead *P*-value below 5×10^{-8}. For the HLA locus, we used a GCTA *P*-value threshold of 5×10^{-8}. We also retained the loci *TSPOAP1*, *IKZF1*, and *TMEM163* since they had $P < 5 \times 10^{-8}$ in an earlier version of our analysis. We excluded the *APOE* locus from conditional analysis and fine-mapping because the strength of association in the region would require a more perfect LD panel match to avoid spurious signals.

We then ran FINEMAP (v1.3) at each locus, with --n-causal-snps given as the number of independent SNPs determined by GCTA. For FINEMAP, we excluded variants with MAF < 0.2%. For loci with multiple signals, we also used GCTA --cojo-cond to condition on each independent SNP identified in the previous analysis, and retained SNPs within 500 kb of any conditionally independent SNP at the locus. To fine-map based on GCTA conditional signals, we converted beta and standard error values to approximate Bayes Factors (BF)[101] using a prior of W = 0.1 (in Wakefield notation), and used the WTCCC single-causal variant method[48], probability = SNP BF / sum(all SNP BFs).

To assess sensitivity of the results to our choice of reference panel, we applied the same steps (GCTA + FINEMAP) to summary statistics from the Kunkle et al. sub-study, which are described further in the Supplementary Note.

Colocalization with eQTLs

For eQTL colocalization, we downloaded summary statistics (see URLs) and determined eQTL genes at FDR 5% for each dataset in a uniform manner, first using Bonferroni correction of lead SNP nominal *P* values based on the number of variants tested for the gene, and using the Benjamini-Hochberg method to compute FDR. QTL calling for primary microglia was performed with RASQUAL[102] with the --no-posterior-update option. For datasets in GRCh38 coordinates, we first used CrossMap[100] to convert back to GRCh37 coordinates to match variants between eQTL and GWAS. We used the coloc package[19] with default priors to perform colocalization tests between GWAS and eQTLs having lead variants within 500 kb of each other, and passed to coloc all variants within 200 kb of each lead variant. We also ran coloc using *P*-values for each conditionally independent GWAS signal, obtained with GCTA as described above.

Functional annotations

We used the Ensembl VEP online Web tool (www.ensembl.org/vep)[55] to predict variant consequences, and to add selected annotations (Supplementary Table 7). We downloaded bed files based on imputed data for Roadmap Epigenomics DNase and 25-state genome segmentations for 127 epigenomes[54]. We grouped these into groups “all”, “brain” (epigenomes 7, 9, 10, 53, 54, 67, 68, 69, 70, 71, 72, 73, 74, 81, 82, 125), and “blood & immune” (epigenomes 33, 34, 37, 38, 39, 40, 41, 42, 43, 44, 45, 47, 48, 62, 29, 30, 31, 32, 35, 36, 46, 50, 51, 116). We considered 9 genome segmentation states to represent enhancers: TxReg, TxEnh5, TxEnh3, TxEnhW, EnhA1, EnhA2, EnhAF, EnhW1, EnhW2. We used bedtools[103] to determine overlaps, and counted the number of overlaps for each variant with peaks in the above groups. We downloaded FANTOM5[104] permissive enhancer annotations from fantom.gsc.riken.jp/5/data/. We downloaded pre-computed SpliceAI scores[58] for variants within genes from github.com/Illumina/SpliceAI. We merged filtered whole-genome and exome scores together, and for each AD variant annotated the maximum score across splice donor gain, donor loss, acceptor gain, acceptor loss. We used DeepSEA[57] (deepsea.princeton.edu) to annotate variants selected for functional fine-mapping with DeepSEA’s “functional significance” score. BigWig files with PhastCons, PhyloP and GERP RS scores were downloaded from UCSC. We downloaded microglial ATAC-seq based on the study by Gosselin et al.[52], aligned reads to GRCh37 with bwa 0.7.15[105], and called multisample peaks across all 15 datasets using MACS2[106]. We prepared bigWig files from alignments by using bedtools genomecov, followed by bedGraphToBigWig. To visualise microglia ATAC-seq tracks we adapted code from wiggleplotr[107].

Annotation-based fine-mapping

For fine-mapping with PAINTOR, we first restricted the number of considered variants for computational feasibility, by selecting 3,207 variants which had (i) FINEMAP probability ≥ 0.01% based on the GCTA-identified number of causal variants at the locus, or (ii) had FINEMAP probability ≥ 1% when run with either 1 or 2 causal variants, or (iii) were among the top 20 variants at the locus by FINEMAP probability. We defined binary annotations for input to PAINTOR based on the features described above, thresholding certain scores at multiple levels (e.g. CADD ≥ 5, 10, 20). For Roadmap annotations, we included a category

based on whether a variant was in a peak or enhancer in ≥ 10 epigenomes. We ran PAINTOR v3.1 once for each of the 43 annotations (Fig. 2 and Supplementary Table 7), allowing two causal variants per locus.

We built a multi-annotation model using forward stepwise selection. We selected the best annotation by log-likelihood (LLK), Blood & immune DNase, and then ran PAINTOR again for each combination of this annotation and the 42 remaining annotations. We added a top-ranking annotation at each iteration until the model LLK improvement was less than 1. This occurred at iteration 4, and so we kept the first three annotations in the combined model. We computed the mean causal probability for each SNP as the mean of the three fine-mapping methods at loci with two or more signals, or as the mean of the FINEMAP and PAINTOR probabilities for loci with one signal, since FINEMAP gives approximately the same results as WTCCC fine-mapping for a single causal variant.

Network analysis

For network analysis, we created a gene interaction network based on selecting all edges between protein-coding genes from systematic studies (>1,000 interactions) in the IntAct[108] and BioGRID databases[109], and edges from STRING v10.5[110] with edge score > 0.75. This combined network included 18,055 genes and 540,421 edges. We identified 28 top candidate genes across AD loci (Supplementary Table 9) to use as seed genes, and assigned weight to these as the $-\log_{10}(P\text{ value})$ of the locus lead SNP. We added four genes from the literature (*MAPT*, *PSEN1*, *PSEN2*, *ABI3*), with a weight (equivalent $-\log_{10}(P)$) of 15. For three loci, the nearest gene was not present in the network (*ECHDC3*, *TMEM163*, *SCIMP*). For each locus, we used all seed genes as input except those at the same locus, and propagated information through the network with the personalized PageRank algorithm[111], included in the igraph R package[112]. Since a gene's resulting PageRank was highly correlated with its node degree, we compared the PageRank of each gene to the distribution of PageRanks obtained for the same gene in 1,000 iterations of network propagation, where the same number of seed genes were randomly selected. We computed the percentile of a gene's true PageRank relative to the 1,000 network propagations with randomized inputs. Although the distribution of PageRank percentile was fairly uniform, we further normalised this to a uniform distribution across genes, so that a Pagerank percentile of 90% indicates that a gene's PageRank relative to permutations is above that of 90% of genes. To determine gene set enrichment, we used the top 1,000 genes by network rank as input to gProfiler[113] with default settings, with the set of all genes ranked by the network as a background set. To determine enrichment of low *P*-value AD SNPs near genes in specific bins of PageRank percentile (Fig. 5a), we first determined for each gene the minimum SNP *P* value within 10 kb of the gene's footprint. We excluded genes within 1 Mb of *APOE*. Then, for genes in each PageRank percentile bin, we used Fisher's exact test to determine the odds ratio for a gene in that bin (relative to genes with PageRank percentile <50%) to have a minimum SNP *P* value in the given bin (relative to genes with minimum SNP $P > 0.01$).

Gene expression

Gene expression values for all tissues were determined in units of transcripts per million (TPM). Both GTEx v8 and the eQTL catalogue provide tables of the median TPM

expression across samples for each tissue and gene. For primary microglia, we obtained a table of read counts per gene, computed using FeatureCounts 1.5.3 as described[14], from which we computed median TPM. For use in gene prioritization and enrichment analyses, we first selected four GTEx brain tissues (cortex, hippocampus, substantia nigra, cerebellum) to avoid over-representing brain, and then the remaining 41 GTEx tissues, as well primary microglia and in-house expression data from iPSC-derived microglia, iPSC-derived NGN2 cortical neurons, and iPSC-derived neurons from growth factor differentiation. For each gene, we determined the TPM expression relative to all tissues/cell types.

Single-cell gene expression data were obtained from the Allen Brain Institute as a gene-by-cell counts table, based on Smart-seq profiling of six human brain cortical areas[77]. For each cell type "subclass" as defined in the metadata (but excluding VLMC for having too few cells, and the outlier subclass labelled "exclude"), counts were summed across cells and then normalised to TPM within each subclass. We determined each gene's TPM expression in each subclass relative to all 18 subclasses.

Genome-wide enrichment

We determined the GRCh37 coordinates of 18,055 genes present in the gene network using the R package annotables 0.1.91. For each AD GWAS SNP, excluding the *APOE* region (chr19:44-47 Mb), we determined the nearest gene. We defined annotation inputs for fgwas labelling a SNP 1 if it was nearest to a gene with network score in a given percentile bin (50-60, 60-70, 70-80, 80-90, 90-95, >95) and 0 otherwise. We ran fgwas[78] (-cc) with all network annotations as input, so that enrichments are with respect to SNPs nearest to genes with network score < 50th percentile. For every bulk gene expression dataset selected above, we defined an annotation for SNPs nearest genes with relative expression above the 80th (or 90th) percentile, and similarly for cell types from single-cell gene expression. We ran fgwas once for each expression annotation to determine enrichment of SNPs near high-expression genes relative to remaining genes (Supplementary Table 12).

Gene prioritization

Five predictors were used for gene prioritization.

The **coding score** is the sum of the mean fine-mapping probability for missense or LoF variants in a gene.

The **expression score** is the sum of component scores for bulk and single-cell microglial expression, and rewards genes with expression percentile above the 50th:

$$\begin{aligned}\text{exprScore} &= (\text{bulkExprscore} + \text{singleCellExprscore})/2\\ \text{bulkExprScore} &= \max(0, \text{bulk\_microglia\_pctile-50})/50\\ \text{singleCellExprScore} &= \max(0, \text{sc\_microglia\_pctile-50})/50\end{aligned}$$

Genes without measured expression in a given dataset (bulk, single-cell) are assigned an exprScore of zero for that dataset.

Recent evidence from both eQTLs[114] and metabolite GWAS[115] suggests that genomic distance from the association peak is a strong predictor of causal target genes. The **distance score** is defined to give reasonable scores over the main range of interest of 0 - 200 kb:

$$\text{distScore} = (\log10(\max \text{Dist}) - \log10((abs(x) + \text{distBias}))) / (\log10(\text{maxDist}) - \log10(\text{distBias}))$$

where x is the minimum distance from the gene's footprint to the region defined by independent lead SNPs at a GWAS locus, maxDist is 500,000 and distBias is 100 (Extended Data Fig. 6).

The **coloc score** is defined based on the maximum value across QTL datasets of the "H4" hypothesis probability, and rewards colocalisation probabilities above 0.9:

$$\text{colocScore} = \max(0, \max(\text{QTL dataset H4}) - 0.9)$$

The **network score** is determined based on the pagerank percentile for a gene relative to permutations:

$$\text{networkScore} = \max(0, (\text{pagerank pctile} - 50)/50)$$

Genes not present in the network are assigned a networkScore of zero.

The **total score** for a gene is the sum of the above five scores.

To give appropriate weight to each component, we trained lasso-regularized logistic regression models with cross-validation using glmnet[116]. As input we used all protein-coding genes within 500 kb of our AD GWAS peaks, excluding the *APOE* region due to lack of colocalisation information, and excluding genes not present in the network. For the distance model, genes within 10 kb of each GWAS peak (40 genes) were set as positives, genes 10-100 kb were excluded, and genes >100 kb (394 genes) were set as negatives. These were predicted using the four non-distance predictors. For the network model, genes with pagerank percentile >80% (143 genes) were set as positives, those with pagerank percentile 50-80% were excluded, the 230 other genes were set as negatives, and these were predicted using the four non-network predictors. In each case, we selected the model that minimized mean squared error (MSE), shown in Supplementary Table 14, and used those parameters to generate predictions (in the range 0-1) for all genes at the AD loci. We defined the **model score** for a gene as the average prediction from the two models. To determine the importance of the predictors to each model (apart from looking at regression coefficients) we ran glmnet models excluding each predictor in turn. If the MSE was lower with a predictor excluded then we removed it from the final model. For each model, we compared the MSE when using our quantitative predictors as defined above, or using categorical predictors by thresholding the predictors into 2-4 bins. For both models, the quantitative predictors gave improved MSE. We also examined models that included as predictors expression scores from astrocytes (based on the single-cell data) and from brain hippocampus (based on the GTEx data), but for both models this resulted in higher MSE and the regularization set the coefficients to zero.

Europe PMC Funders Author Manuscripts

Extended Data

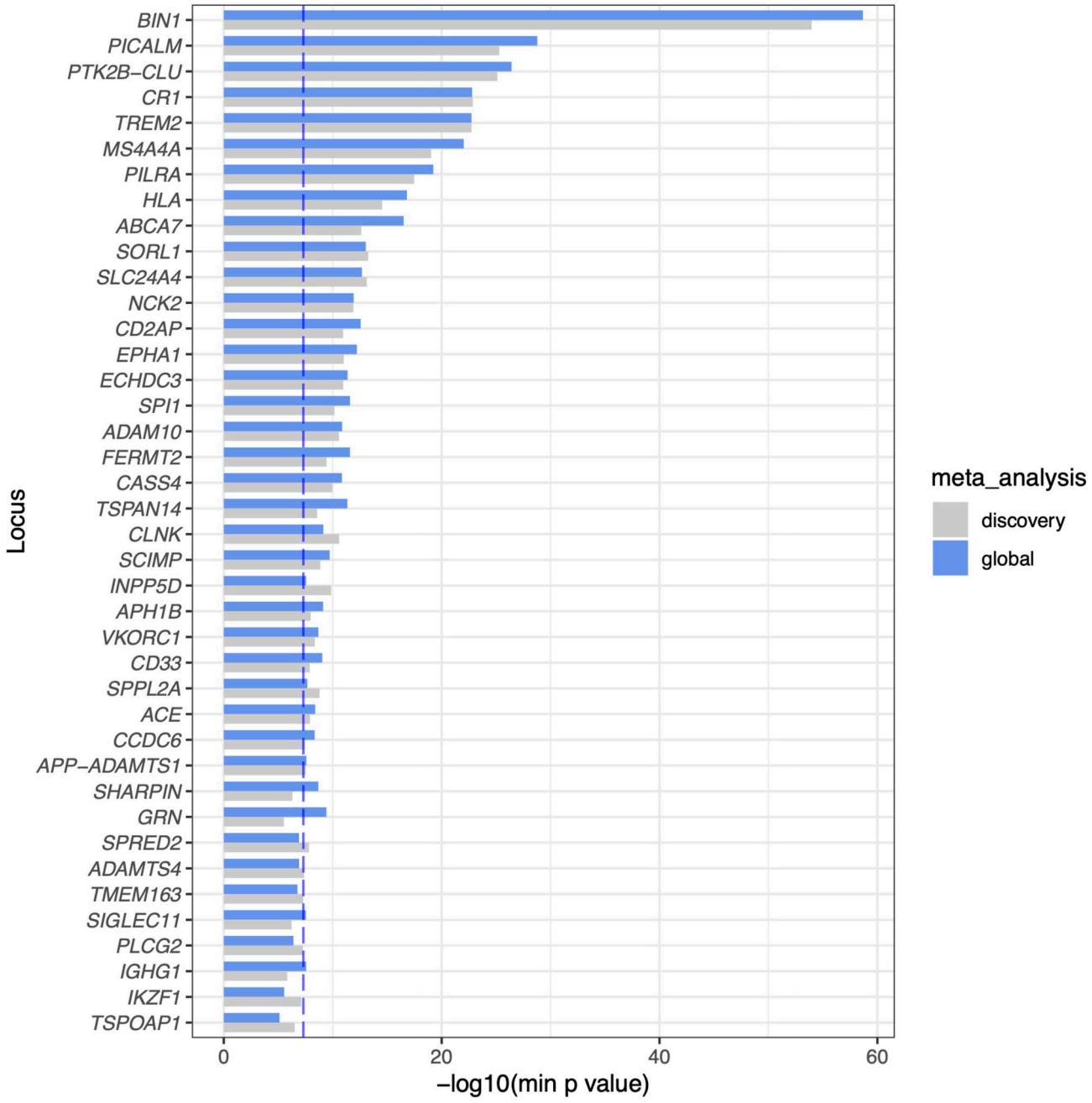

Extended Data Fig. 1. Association of AD loci in discovery + replication ("global") meta-analysis

Association of AD loci in discovery + replication dataset ("global") meta-analysis. For most loci, association significance is increased in the global meta-analysis (blue bars) relative to the discovery analysis (grey bars). The dashed vertical line shows $P = 5 \times 10^{-8}$. *P*-values were computed by inverse variance weighted meta-analysis, and bars show the $-\log_{10}(P)$ for the SNP with minimum *P* value at the locus in either the discovery or global meta-analysis.

Europe PMC Funders Author Manuscripts

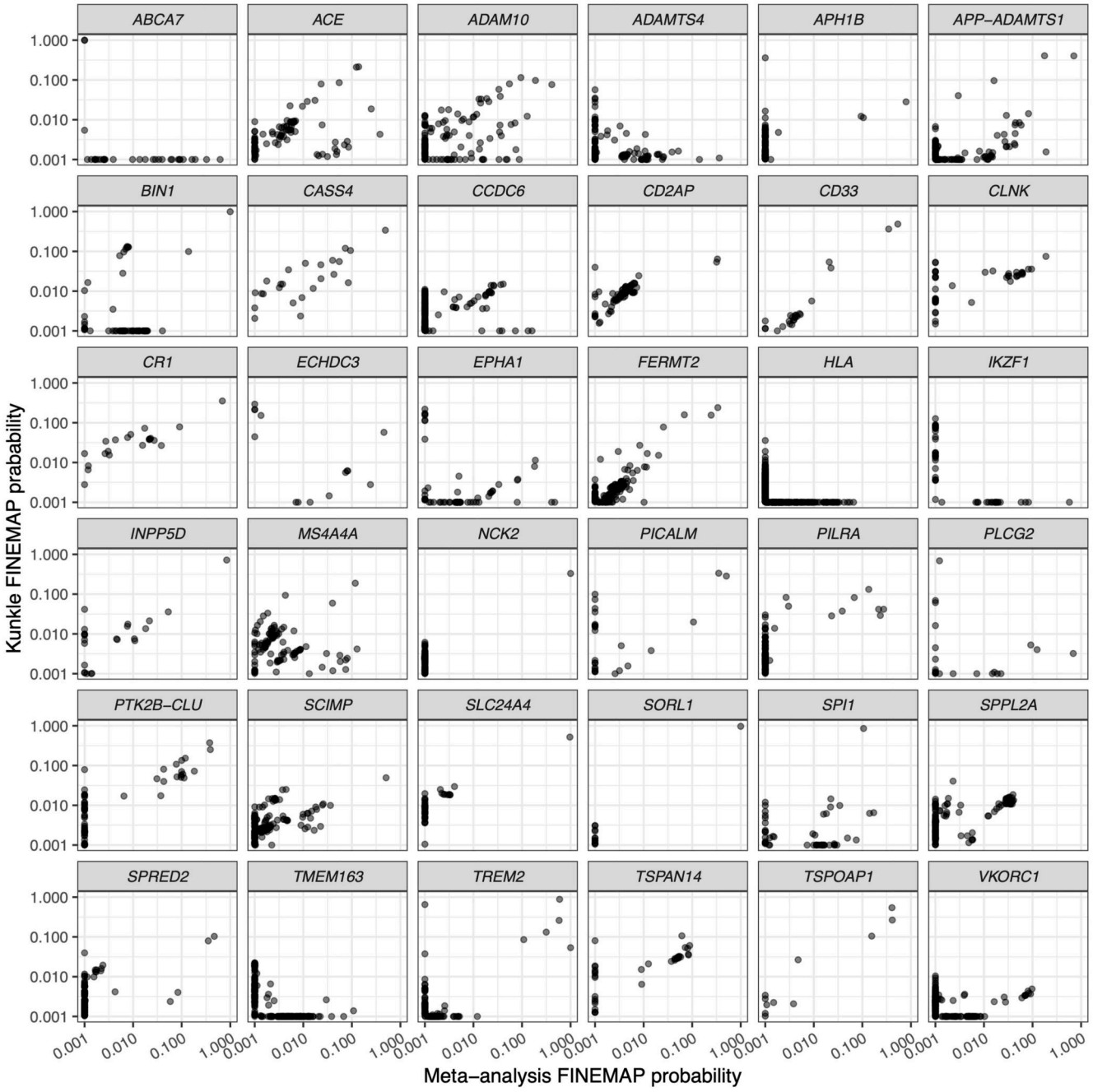

Extended Data Fig. 2. Comparison of fine-mapping in the meta-analysis vs. Kunkle et al.

Comparison of fine-mapping in the meta-analysis vs. Kunkle et al. Scatterplots showing, for each locus, SNP probabilities from FINEMAP applied to either the Kunkle et al. + UK Biobank meta-analysis (*x*-axis), or to only Kunkle et al. The number of causal variants at each locus was set to the number detected by GCTA in the meta-analysis. For most of the 36 loci, SNP probabilities are well correlated. For a few loci that are well powered in Kunkle et al., this is not the case, namely *ABCA7, EPHA1, ECHDC3*, and *HLA*. For these loci, fine-mapping results should be interpreted with caution. Six other loci are not well correlated

(*ADAMTS4*, *APH1B*, *IKZF1*, *PLCG2*, *TMEM163*, and *VKORC1*), but these loci are poorly powered in Kunkle et al. (lead *P* values 2.1 x 10^{-6} to 2.1 x 10^{-3}).

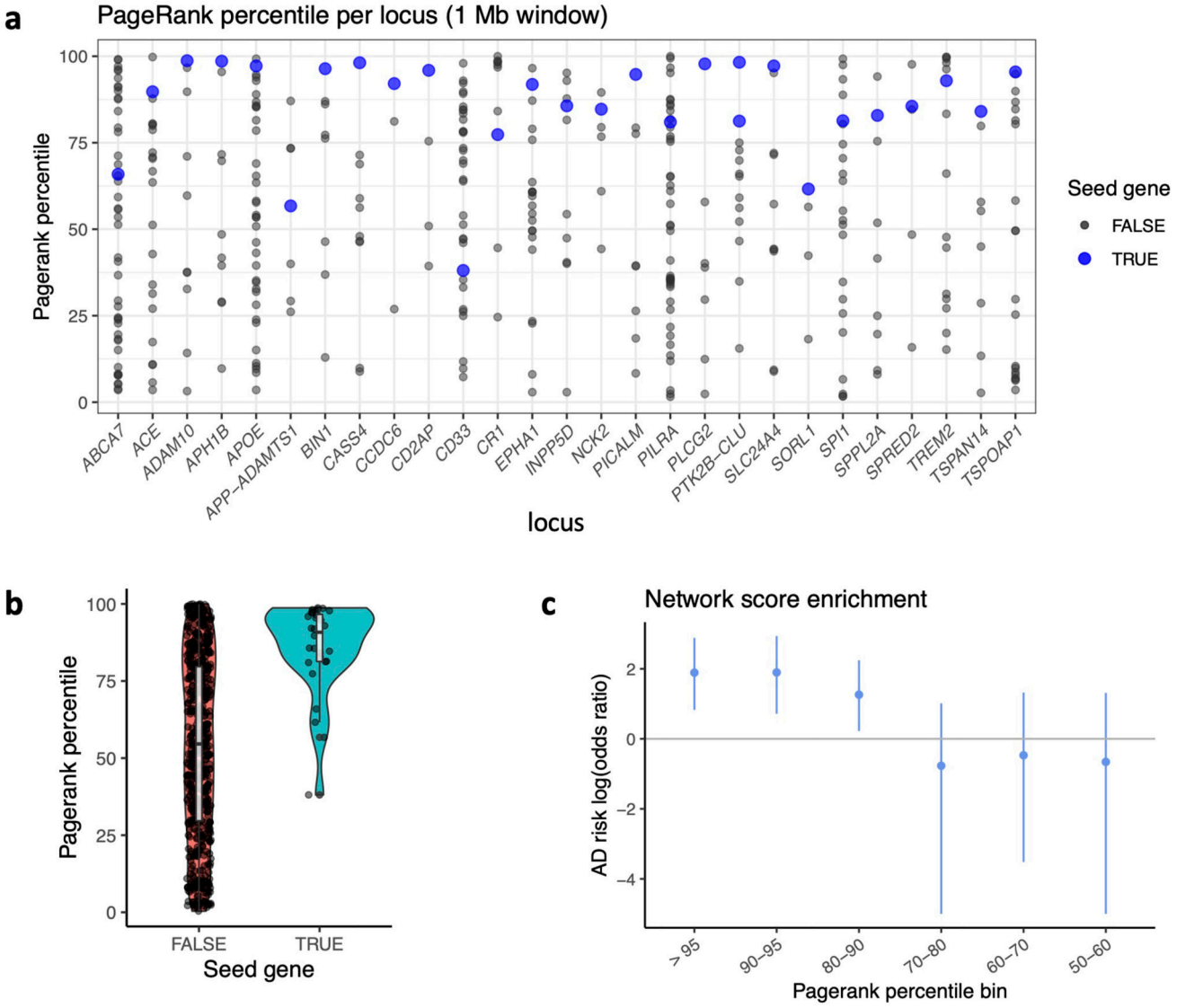

Extended Data Fig. 3. Network enrichment

a, The Pagerank percentile of all genes (within 500 kb) at each AD GWAS locus containing a seed gene is shown, with seed genes highlighted in blue. **b**, A violin/boxplot shows that seed genes have a markedly higher network Pagerank percentile than remaining genes (*P* = 2.4 x 10^{-9}, one-tailed Wilcoxon rank sum test). **c**, Log odds ratio enrichment of AD risk among SNPs nearest to genes with network Pagerank percentile in different bins, determined using fgwas (whiskers represent 95% confidence intervals).

Europe PMC Funders Author Manuscripts

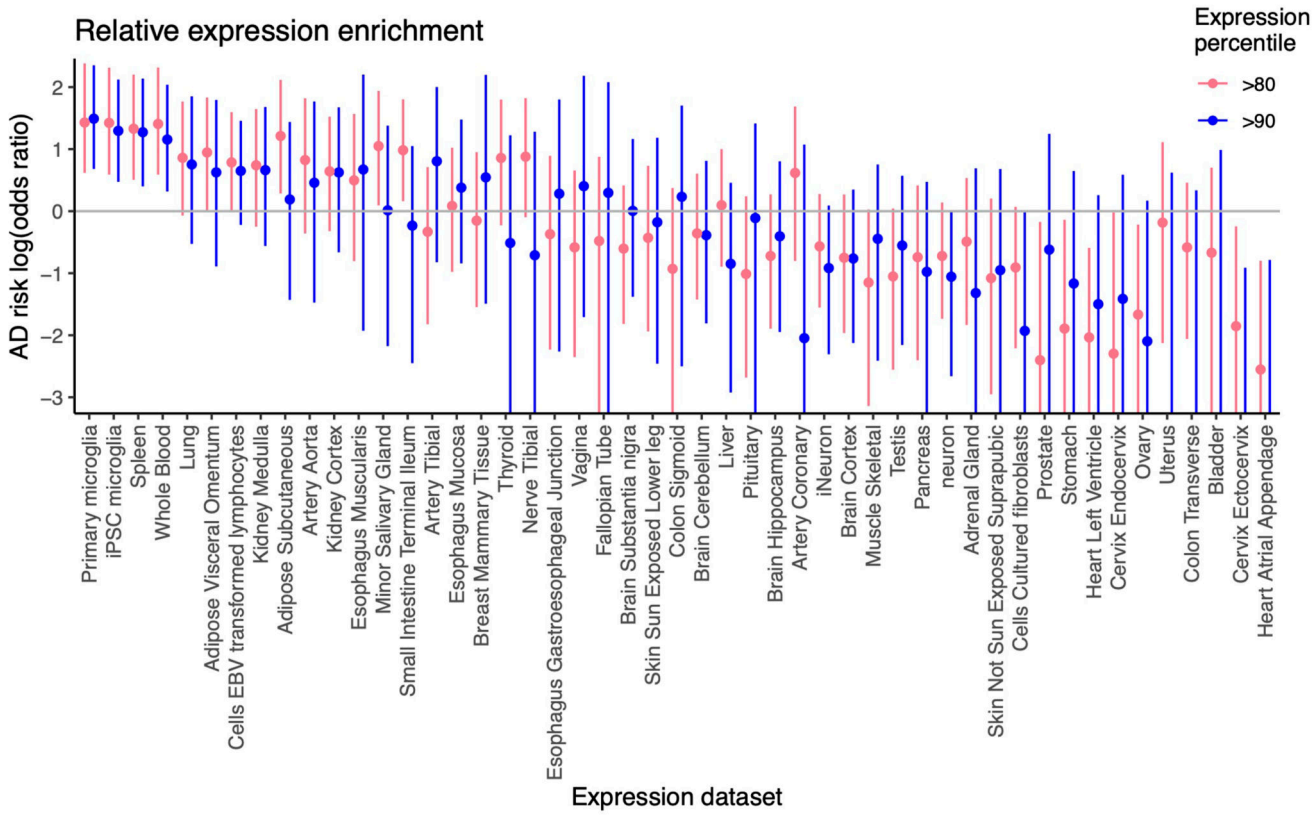

Extended Data Fig. 4. Gene expression enrichments

Expression enrichments for GTEx + microglia. Shown are the log odds ratio enrichments of AD risk among SNPs with relative gene expression in each tissue above the 80th (or 90th) percentile across tissues. Whiskers represent 95% confidence intervals determined by fgwas.

Europe PMC Funders Author Manuscripts

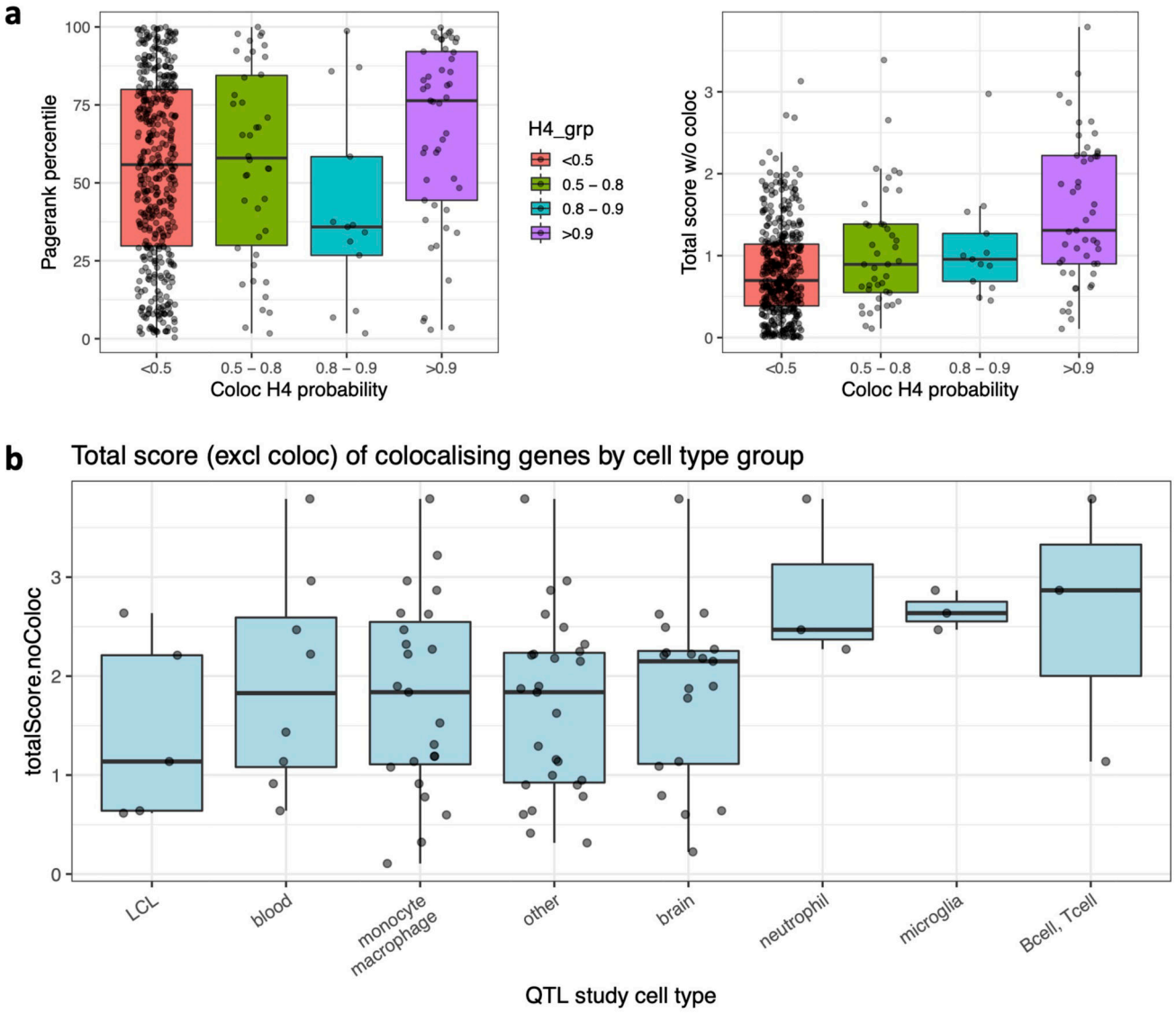

Extended Data Fig. 5. Colocalization scores

a, Genes with maximum colocalization H4 probability >0.9 have higher Pagerank percentile (left boxplot) and higher total score (sum of the four non-coloc predictors, right boxplot) than do genes without colocalisation (<0.5). Genes with intermediate colocalisation evidence (bins 0.5 - 0.8 and 0.8 - 0.9) show little evidence of having higher scores by the other metrics. Based on this, we chose a maxColoc probability of 0.9 as the lower bound for our colocalization score. **b**, Boxplot of the total score (excluding coloc) for genes that have a colocalisation probability > 0.9 in at least one QTL dataset within each tissue group. The most significant difference is between totalScore for genes with microglial colocalizations vs. the genes with colocalization in “other” tissues (non-immune GTEx tissues), but the for a difference is weak ($P = 0.041$, Wilcoxon rank sum test). In all cases, boxplots show the 25th, median, and 75th percentile of the distribution, with whiskers extending to the largest (and smallest) value no further than 1.5 times the interquartile range from the boxplot hinge.

Europe PMC Funders Author Manuscripts

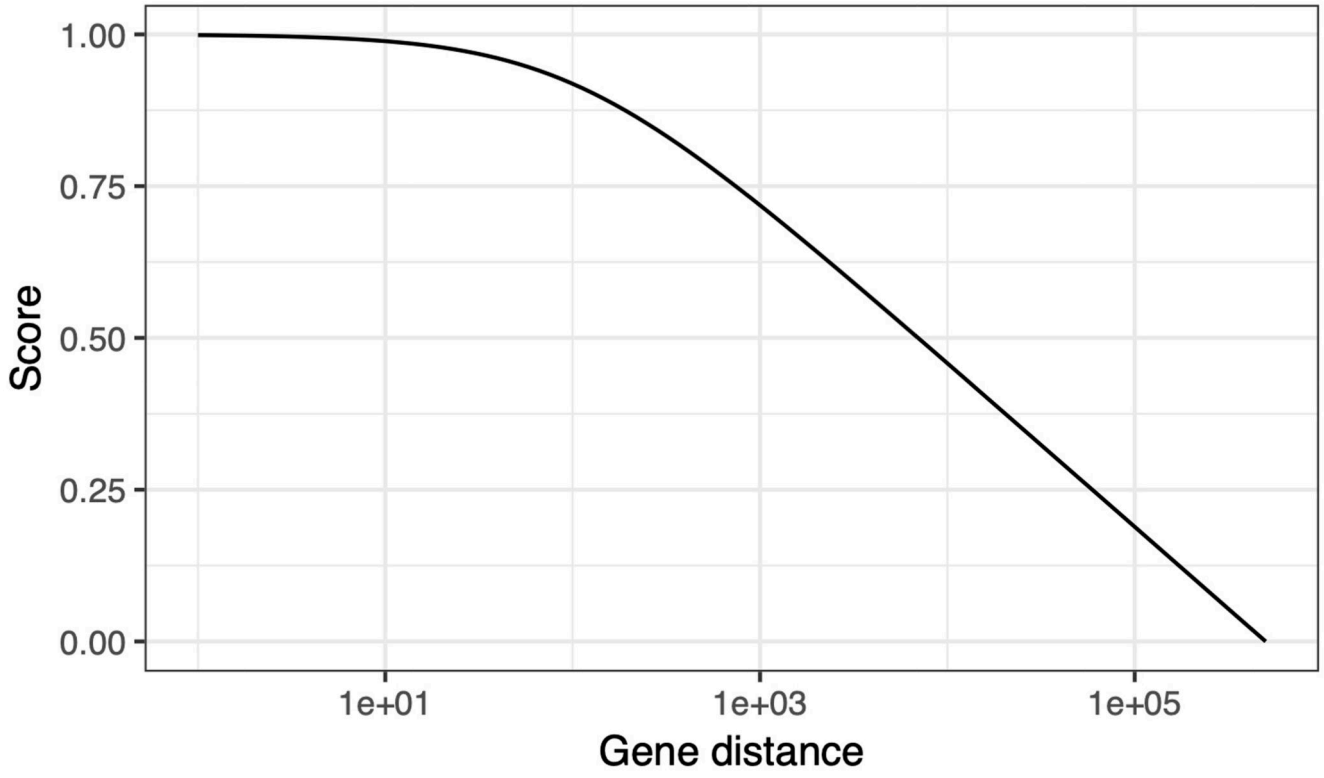

Extended Data Fig. 6. Gene distance score

The distance score assigned to genes near an AD GWAS peak, which decreases approximately linearly (past a distance of 1 kb) with increasing log-scaled distance up to 500 kb.

Supplementary Material

Refer to Web version on PubMed Central for supplementary material.

Acknowledgements

This work was funded by Open Targets (OTAR037). We thank Jeff Barrett for guidance during initiation of the project, and Kaur Alasoo for early access to the eQTL catalogue. We thank Agustín Ruiz for support in using summary results from the Gr@ace study. We acknowledge the participants and investigators of FinnGen study, and of the UK Biobank. R.J.M.F. is supported by grants from the UK Multiple Sclerosis Society (MS 50), the Adelson Medical Research Foundation, and a core support grant from Wellcome and MRC to the Wellcome-MRC Cambridge Stem Cell Institute (203151/Z/16/Z). A.M.H.Y. is supported by a Wellcome Trust PhD for Clinicians fellowship.

Data availability

Summary statistics from the meta-analysis are available through the NHGRI-EBI GWAS Catalog under accessions GCST90012877 and GCST90012878:

www.ebi.ac.uk/gwas/downloads/summary-statistics

eQTL Catalogue: www.ebi.ac.uk/eqtl

GTEx: www.gtexportal.org

Roadmap Epigenomics: www.roadmapepigenomics.org

DeepSEA: deepsea.princeton.edu

SpliceAI: github.com/Illumina/SpliceAI

FANTOM enhancers: fantom.gsc.riken.jp/5/data/

GERP: hgdownload.cse.ucsc.edu/gbdb/hg19/bbi/All_hg19_RS.bw

PhyloP: hgdownload.cse.ucsc.edu/goldenpath/hg19/phyloP100way

PhastCons: hgdownload.cse.ucsc.edu/goldenpath/hg19/phastCons100way

Brain eQTL meta-analysis summary statistics: www.synapse.org/#!Synapse:syn16984815

Primary microglia eQTL summary statistics, EGA Accession ID: EGAD00001005736

Primary microglia ATAC-seq, dbGaP Study Accession: phs001373.v1.p1

Allen Brain Institute: portal.brain-map.org/atlases-and-data/rnaseq

IntAct database: www.ebi.ac.uk/intact

BioGRID database: thebiogrid.org

STRING database: string-db.org

Code availability

Code for analyses described here can be found at github.com/jeremy37/AD_finemap.

References

1. Liu JZ, Erlich Y, Pickrell JK. Case-control association mapping by proxy using family history of disease. Nat Genet. 2017; 49:325–331. [PubMed: 28092683]
2. Marioni RE, et al. GWAS on family history of Alzheimer's disease. Transl Psychiatry. 2018; 8:99. [PubMed: 29777097]
3. Jansen IE, et al. Genome-wide meta-analysis identifies new loci and functional pathways influencing Alzheimer's disease risk. Nat Genet. 2019; 51:404–413. [PubMed: 30617256]
4. Claussnitzer M, et al. FTO obesity variant circuitry and adipocyte browning in humans. N Engl J Med. 2015; 373:895–907. [PubMed: 26287746]
5. Sekar A, et al. Schizophrenia risk from complex variation of complement component 4. Nature. 2016; 530:177–183. [PubMed: 26814963]
6. Huang H, et al. Fine-mapping inflammatory bowel disease loci to single-variant resolution. Nature. 2017; 547:173–178. [PubMed: 28658209]
7. Malik M, et al. CD33 Alzheimer's risk-altering polymorphism, CD33 expression, and exon 2 splicing. J Neurosci. 2013; 33:13320–13325. [PubMed: 23946390]
8. Guerreiro R, et al. TREM2 variants in Alzheimer's disease. N Engl J Med. 2013; 368:117–127. [PubMed: 23150934]

9. Sims R, et al. Rare coding variants in PLCG2, ABI3, and TREM2 implicate microglial-mediated innate immunity in Alzheimer's disease. Nat Genet. 2017; 49:1373–1384. [PubMed: 28714976]
10. Kerimov N, et al. eQTL Catalogue: a compendium of uniformly processed human gene expression and splicing QTLs. bioRxiv. 2020; doi: 10.1101/2020.01.29.924266
11. GTEx Consortium. The GTEx Consortium atlas of genetic regulatory effects across human tissues. Science. 2020; 369:1318–1330. [PubMed: 32913098]
12. Kunkle BW, et al. Genetic meta-analysis of diagnosed Alzheimer's disease identifies new risk loci and implicates Aβ, tau, immunity and lipid processing. Nat Genet. 2019; 51:414–430. [PubMed: 30820047]
13. Lambert JC, et al. Meta-analysis of 74,046 individuals identifies 11 new susceptibility loci for Alzheimer's disease. Nat Genet. 2013; 45:1452–1458. [PubMed: 24162737]
14. Young AMH, et al. A map of transcriptional heterogeneity and regulatory variation in human microglia. bioRxiv. 2019; doi: 10.1101/2019.12.20.874099
15. Leung YY, et al. Identifying amyloid pathology–related cerebrospinal fluid biomarkers for Alzheimer's disease in a multicohort study. Alzheimers Dement. 2015; 1:339–348.
16. Bulik-Sullivan BK, et al. LD Score regression distinguishes confounding from polygenicity in genome-wide association studies. Nat Genet. 2015; 47:291–295. [PubMed: 25642630]
17. Moreno-Grau S, et al. Genome-wide association analysis of dementia and its clinical endophenotypes reveal novel loci associated with Alzheimer's disease and three causality networks: The GR@ACE project. Alzheimers Dement. 2019; 15:1333–1347. [PubMed: 31473137]
18. Yang J, et al. Conditional and joint multiple-SNP analysis of GWAS summary statistics identifies additional variants influencing complex traits. Nat Genet. 2012; 44:369–75. [PubMed: 22426310]
19. Giambartolomei C, et al. Bayesian test for colocalisation between pairs of genetic association studies using summary statistics. PLoS Genet. 2014; 10:e1004383. [PubMed: 24830394]
20. Sieberts SK, et al. Large eQTL meta-analysis reveals differing patterns between cerebral cortical and cerebellar brain regions. Sci Data. 2020; 7:340. [PubMed: 33046718]
21. Ng B, et al. An xQTL map integrates the genetic architecture of the human brain's transcriptome and epigenome. Nat Neurosci. 2017; 20:1418–1426. [PubMed: 28869584]
22. Schmiedel BJ, et al. Impact of genetic polymorphisms on human immune cell gene expression. Cell. 2018; 175:1701–1715.e16. [PubMed: 30449622]
23. Jaffe AE, et al. Developmental and genetic regulation of the human cortex transcriptome illuminate schizophrenia pathogenesis. Nat Neurosci. 2018; 21:1117–1125. [PubMed: 30050107]
24. Buil A, et al. Gene-gene and gene-environment interactions detected by transcriptome sequence analysis in twins. Nat Genet. 2015; 47:88–91. [PubMed: 25436857]
25. Fairfax BP, et al. Genetics of gene expression in primary immune cells identifies cell type–specific master regulators and roles of HLA alleles. Nat Genet. 2012; 44:502–510. [PubMed: 22446964]
26. Fairfax BP, et al. Innate immune activity conditions the effect of regulatory variants upon monocyte gene expression. Science. 2014; 343
27. Naranbhai V, et al. Genomic modulators of gene expression in human neutrophils. Nat Commun. 2015; 6:7545. [PubMed: 26151758]
28. Chen L, et al. Genetic drivers of epigenetic and transcriptional variation in human immune cells. Cell. 2016; 167:1398–141.e24. [PubMed: 27863251]
29. Alasoo K, et al. Shared genetic effects on chromatin and gene expression indicate a role for enhancer priming in immune response. Nat Genet. 2018; 50:424–431. [PubMed: 29379200]
30. Gutierrez-Arcelus M, et al. Passive and active DNA methylation and the interplay with genetic variation in gene regulation. Elife. 2013; 2:e00523. [PubMed: 23755361]
31. Lappalainen T, et al. Transcriptome and genome sequencing uncovers functional variation in humans. Nature. 2013; 501:506–511. [PubMed: 24037378]
32. Kilpinen H, et al. Common genetic variation drives molecular heterogeneity in human iPSCs. Nature. 2017; 546:370–375. [PubMed: 28489815]
33. Nédélec Y, et al. Genetic ancestry and natural selection drive population differences in immune responses to pathogens. Cell. 2016; 167:657–669.e21. [PubMed: 27768889]

34. Quach H, et al. Genetic adaptation and Neandertal admixture shaped the immune system of human populations. Cell. 2016; 167:643–656.e17. [PubMed: 27768888]
35. Schwartzentruber J, et al. Molecular and functional variation in iPSC-derived sensory neurons. Nat Genet. 2018; 50:54–61. [PubMed: 29229984]
36. van de Bunt M, et al. Transcript expression data from human islets links regulatory signals from genome-wide association studies for type 2 diabetes and glycemic traits to their downstream effectors. PLoS Genet. 2015; 11:e1005694. [PubMed: 26624892]
37. Momozawa Y, et al. IBD risk loci are enriched in multigenic regulatory modules encompassing putative causative genes. Nat Commun. 2018; 9:2427. [PubMed: 29930244]
38. Chun S, et al. Limited statistical evidence for shared genetic effects of eQTLs and autoimmune-disease-associated loci in three major immune-cell types. Nat Genet. 2017; 49:600–605. [PubMed: 28218759]
39. Salazar SV, et al. Alzheimer's disease risk factor Pyk2 mediates amyloid-β-induced synaptic dysfunction and loss. J Neurosci. 2019; 39:758–772. [PubMed: 30518596]
40. Raj T, et al. Integrative transcriptome analyses of the aging brain implicate altered splicing in Alzheimer's disease susceptibility. Nat Genet. 2018; 50:1584–1592. [PubMed: 30297968]
41. Calafate S, Flavin W, Verstreken P, Moechars D. Loss of Bin1 promotes the propagation of Tau pathology. Cell Rep. 2016; 17:931–940. [PubMed: 27760323]
42. Nott A, et al. Brain cell type–specific enhancer–promoter interactome maps and disease-risk association. Science. 2019; 366:1134–1139. [PubMed: 31727856]
43. Rathore N, et al. Paired Immunoglobulin-like Type 2 Receptor Alpha G78R variant alters ligand binding and confers protection to Alzheimer's disease. PLoS Genet. 2018; 14:e1007427. [PubMed: 30388101]
44. Chan G, et al. CD33 modulates TREM2: convergence of Alzheimer loci. Nat Neurosci. 2015; 18:1556–1558. [PubMed: 26414614]
45. Raj T, et al. CD33: increased inclusion of exon 2 implicates the Ig V-set domain in Alzheimer's disease susceptibility. Hum Mol Genet. 2014; 23:2729–2736. [PubMed: 24381305]
46. Jonsson T, et al. Variant of TREM2 associated with the risk of Alzheimer's disease. N Engl J Med. 2013; 368:107–116. [PubMed: 23150908]
47. Claes C, et al. Human stem cell-derived monocytes and microglia-like cells reveal impaired amyloid plaque clearance upon heterozygous or homozygous loss of TREM2. Alzheimers Dement. 2019; 15:453–464. [PubMed: 30442540]
48. Wellcome Trust Case Control Consortium. et al. Bayesian refinement of association signals for 14 loci in 3 common diseases. Nat Genet. 2012; 44:1294–1301. [PubMed: 23104008]
49. Benner C, et al. FINEMAP: efficient variable selection using summary data from genome-wide association studies. Bioinformatics. 2016; 32:1493–1501. [PubMed: 26773131]
50. Kichaev G, et al. Integrating functional data to prioritize causal variants in statistical fine-mapping studies. PLoS Genet. 2014; 10:e1004722. [PubMed: 25357204]
51. Benner C, et al. Prospects of fine-mapping trait-associated genomic regions by using summary statistics from genome-wide association studies. Am J Hum Genet. 2017; 101:539–551. [PubMed: 28942963]
52. Gosselin D, et al. An environment-dependent transcriptional network specifies human microglia identity. Science. 2017; 356
53. Alasoo K, et al. Shared genetic effects on chromatin and gene expression indicate a role for enhancer priming in immune response. Nat Genet. 2018; 50:424–431. [PubMed: 29379200]
54. Roadmap Epigenomics Consortium. et al. Integrative analysis of 111 reference human epigenomes. Nature. 2015; 518:317–330. [PubMed: 25693563]
55. McLaren W, et al. The Ensembl Variant Effect Predictor. Genome Biol. 2016; 17:122. [PubMed: 27268795]
56. Davydov EV, et al. Identifying a high fraction of the human genome to be under selective constraint using GERP++ PLoS Comput Biol. 2010; 6:e1001025. [PubMed: 21152010]
57. Zhou J, Troyanskaya OG. Predicting effects of noncoding variants with deep learning-based sequence model. Nat Methods. 2015; 12:931–934. [PubMed: 26301843]

58. Jaganathan K, et al. Predicting splicing from primary sequence with deep learning. Cell. 2019; 176:535–548.e24. [PubMed: 30661751]
59. Steinberg S, et al. Loss-of-function variants in ABCA7 confer risk of Alzheimer's disease. Nat Genet. 2015; 47:445–447. [PubMed: 25807283]
60. De Roeck A, et al. An intronic VNTR affects splicing of ABCA7 and increases risk of Alzheimer's disease. Acta Neuropathol. 2018; 135:827–837. [PubMed: 29589097]
61. Bernstein AI, et al. 5-Hydroxymethylation-associated epigenetic modifiers of Alzheimer's disease modulate Tau-induced neurotoxicity. Hum Mol Genet. 2016; 25:2437–2450. [PubMed: 27060332]
62. Witoelar A, et al. Meta-analysis of Alzheimer's disease on 9,751 samples from Norway and IGAP study identifies four risk loci. Sci Rep. 2018; 8:18088. [PubMed: 30591712]
63. Jun GR, et al. Transethnic genome-wide scan identifies novel Alzheimer's disease loci. Alzheimers Dement. 2017; 13:727–738. [PubMed: 28183528]
64. Andersen OM, Rudolph I-M, Willnow TE. Risk factor SORL1: from genetic association to functional validation in Alzheimer's disease. Acta Neuropathol. 2016; 132:653–665. [PubMed: 27638701]
65. Sassi C, et al. Influence of coding variability in APP-Aβ metabolism genes in sporadic Alzheimer's disease. PLoS One. 2016; 11:e0150079. [PubMed: 27249223]
66. Lu Q, et al. Systematic tissue-specific functional annotation of the human genome highlights immune-related DNA elements for late-onset Alzheimer's disease. PLoS Genet. 2017; 13:e1006933. [PubMed: 28742084]
67. Ghanbari M, et al. A functional variant in the miR-142 promoter modulating its expression and conferring risk of Alzheimer disease. Hum Mutat. 2019; 40:2131–2145. [PubMed: 31322790]
68. Chung C-M, et al. Fine-mapping angiotensin-converting enzyme gene: separate QTLs identified for hypertension and for ACE activity. PLoS One. 2013; 8:e56119. [PubMed: 23469169]
69. Nylocks KM, et al. An angiotensin-converting enzyme (ACE) polymorphism may mitigate the effects of angiotensin-pathway medications on posttraumatic stress symptoms. Am J Med Genet B Neuropsychiatr Genet. 2015; 168B:307–315. [PubMed: 25921615]
70. Kamboh MI, et al. Genome-wide association study of Alzheimer's disease. Transl Psychiatry. 2012; 2:e117. [PubMed: 22832961]
71. Canela-Xandri O, Rawlik K, Tenesa A. An atlas of genetic associations in UK Biobank. Nat Genet. 2018; 50:1593–1599. [PubMed: 30349118]
72. Liu JZ, et al. Association analyses identify 38 susceptibility loci for inflammatory bowel disease and highlight shared genetic risk across populations. Nat Genet. 2015; 47:979–986. [PubMed: 26192919]
73. Lanoiselée H-M, et al. APP, PSEN1, and PSEN2 mutations in early-onset Alzheimer disease: A genetic screening study of familial and sporadic cases. PLoS Med. 2017; 14:e1002270. [PubMed: 28350801]
74. Fang H, et al. A genetics-led approach defines the drug target landscape of 30 immune-related traits. Nat Genet. 2019; 51:1082–1091. [PubMed: 31253980]
75. Amin L, Harris DA. Aβ receptors specifically recognize molecular features displayed by fibril ends and neurotoxic oligomers. bioRxiv. 2019; doi: 10.1101/822361
76. Nordestgaard LT, Tybjærg-Hansen A, Nordestgaard BG, Frikke-Schmidt R. Loss-of-function mutation in ABCA1 and risk of Alzheimer's disease and cerebrovascular disease. Alzheimers Dement. 2015; 11:1430–1438. [PubMed: 26079414]
77. Hodge RD, et al. Conserved cell types with divergent features in human versus mouse cortex. Nature. 2019; 573:61–68. [PubMed: 31435019]
78. Pickrell JK. Joint analysis of functional genomic data and genome-wide association studies of 18 human traits. Am JHum Genet. 2014; 94:559–573. [PubMed: 24702953]
79. Bakken TE, et al. Evolution of cellular diversity in primary motor cortex of human, marmoset monkey, and mouse. bioRxiv. 2020; doi: 10.1101/2020.03.31.016972
80. Chang D, et al. A meta-analysis of genome-wide association studies identifies 17 new Parkinson's disease risk loci. Nat Genet. 2017; 49:1511–1516. [PubMed: 28892059]

81. Mukherjee S, Klaus C, Pricop-Jeckstadt M, Miller JA, Struebing FL. A microglial signature directing human aging and neurodegeneration-related gene networks. Front Neurosci. 2019; 13:2. [PubMed: 30733664]
82. Zhang B, et al. Integrated systems approach identifies genetic nodes and networks in late-onset Alzheimer's disease. Cell. 2013; 153:707–720. [PubMed: 23622250]
83. Patel KR, et al. Single cell-type integrative network modeling identified novel microglial-specific targets for the phagosome in Alzheimer's disease. bioRxiv. 2020; doi: 10.1101/2020.06.09.143529
84. Novikova G, et al. Integration of Alzheimer's disease genetics and myeloid genomics reveals novel disease risk mechanisms. bioRxiv. 2019; doi: 10.1101/694281
85. Battle A, et al. Characterizing the genetic basis of transcriptome diversity through RNA-sequencing of 922 individuals. Genome Res. 2014; 24:14–24. [PubMed: 24092820]
86. Biundo F, Ishiwari K, Del Prete D, D'Adamio L. Deletion of the γ-secretase subunits Aph1B/C impairs memory and worsens the deficits of knock-in mice modeling the Alzheimer-like familial Danish dementia. Oncotarget. 2016; 7:11923–11944. [PubMed: 26942869]
87. Nicolas G, et al. Somatic variants in autosomal dominant genes are a rare cause of sporadic Alzheimer's disease. Alzheimers Dement. 2018; 14:1632–1639. [PubMed: 30114415]
88. Zhang X, et al. Negative evidence for a role of APH1B T27I variant in Alzheimer's disease. Hum Mol Genet. 2020; 29:955–966. [PubMed: 31995180]
89. Acx H, et al. Inactivation of γ-secretases leads to accumulation of substrates and non-Alzheimer neurodegeneration. EMBO Mol Med. 2017; 9:1088–1099. [PubMed: 28588032]
90. Matthews AL, et al. Regulation of leukocytes by TspanC8 tetraspanins and the 'molecular scissor' ADAM10. Front Immunol. 2018; 9:1451. [PubMed: 30013551]
91. Schlepckow K, et al. An Alzheimer-associated TREM2 variant occurs at the ADAM cleavage site and affects shedding and phagocytic function. EMBO Mol Med. 2017; 9:1356–1365. [PubMed: 28855300]
92. Ohkura T, et al. Spred2 regulates high fat diet-induced adipose tissue inflammation, and metabolic abnormalities in mice. Front Immunol. 2019; 10:17. [PubMed: 30723473]
93. Juul Rasmussen I, Tybjærg-Hansen A, Rasmussen KL, Nordestgaard BG, Frikke-Schmidt R. Blood-brain barrier transcytosis genes, risk of dementia and stroke: a prospective cohort study of 74,754 individuals. Eur J Epidemiol. 2019; 34:579–590. [PubMed: 30830563]
94. Zhao J, et al. Rare 3-O-sulfation of heparan sulfate enhances Tau interaction and cellular uptake. Angew Chem Int Ed Engl. 2020; 59:1818–1827. [PubMed: 31692167]
95. Bycroft C, et al. The UK Biobank resource with deep phenotyping and genomic data. Nature. 2018; 562:203–209. [PubMed: 30305743]
96. Bellenguez C, et al. A robust clustering algorithm for identifying problematic samples in genome-wide association studies. Bioinformatics. 2012; 28:134–135. [PubMed: 22057162]
97. Manichaikul A, et al. Robust relationship inference in genome-wide association studies. Bioinformatics. 2010; 26:2867–2873. [PubMed: 20926424]
98. Loh P-R, et al. Efficient Bayesian mixed-model analysis increases association power in large cohorts. Nat Genet. 2015; 47:284–290. [PubMed: 25642633]
99. Pirinen M, Donnelly P, Spencer CCA. Efficient computation with a linear mixed model on large-scale data sets with applications to genetic studies. Ann Applied Stat. 2013; 7:369–390.
100. Zhao H, et al. CrossMap: a versatile tool for coordinate conversion between genome assemblies. Bioinformatics. 2014; 30:1006–1007. [PubMed: 24351709]
101. Wakefield J. Bayes factors for genome-wide association studies: comparison with P-values. Genet Epidemiol. 2009; 33:79–86. [PubMed: 18642345]
102. Kumasaka N, Knights AJ, Gaffney DJ. Fine-mapping cellular QTLs with RASQUAL and ATAC-seq. Nat Genet. 2016; 48:206–213. [PubMed: 26656845]
103. Quinlan AR, Hall IM. BEDTools: a flexible suite of utilities for comparing genomic features. Bioinformatics. 2010; 26:841–842. [PubMed: 20110278]
104. Andersson R, et al. An atlas of active enhancers across human cell types and tissues. Nature. 2014; 507:455–461. [PubMed: 24670763]

105. Li H, Durbin R. Fast and accurate long-read alignment with Burrows-Wheeler transform. Bioinformatics. 2010; 26:589–595. [PubMed: 20080505]
106. Zhang Y, et al. Model-based analysis of ChIP-Seq (MACS). Genome Biol. 2008; 9:R137. [PubMed: 18798982]
107. Alasoo K. wiggleplotr: Make read coverage plots from BigWig files. R package version 1101. 2019
108. Orchard S, et al. The MIntAct project—IntAct as a common curation platform for 11 molecular interaction databases. Nucleic Acids Res. 2014; 42:D358–D363. [PubMed: 24234451]
109. Chatr-Aryamontri A, et al. The BioGRID interaction database: 2017 update. Nucleic Acids Res. 2017; 45:D369–D379. [PubMed: 27980099]
110. Szklarczyk D, et al. The STRING database in 2017: quality-controlled protein-protein association networks, made broadly accessible. Nucleic Acids Res. 2017; 45:D362–D368. [PubMed: 27924014]
111. Fogaras D, Rácz B, Csalogány K, Sarlós T. Towards scaling fully personalized PageRank: algorithms, lower bounds, and experiments. Internet Mathematics. 2005; 2:333–358.
112. Csardi G, Nepusz T. The igraph software package for complex network research. Inter Journal, Complex Systems. 2006; 1695:1–9.
113. Raudvere U, et al. g:Profiler: a web server for functional enrichment analysis and conversions of gene lists (2019 update). Nucleic Acids Res. 2019; 47:W191–W198. [PubMed: 31066453]
114. Barbeira AN, et al. Widespread dose-dependent effects of RNA expression and splicing on complex diseases and traits. bioRxiv. 2019; doi: 10.1101/814350
115. Stacey D, et al. ProGeM: a framework for the prioritization of candidate causal genes at molecular quantitative trait loci. Nucleic Acids Res. 2019; 47:e3. [PubMed: 30239796]
116. Friedman J, Hastie T, Tibshirani R. Regularization paths for generalized linear models via coordinate descent. J Stat Softw. 2010; 33:1–22. [PubMed: 20808728]

Europe PMC Funders Author Manuscripts

Europe PMC Funders Author Manuscripts

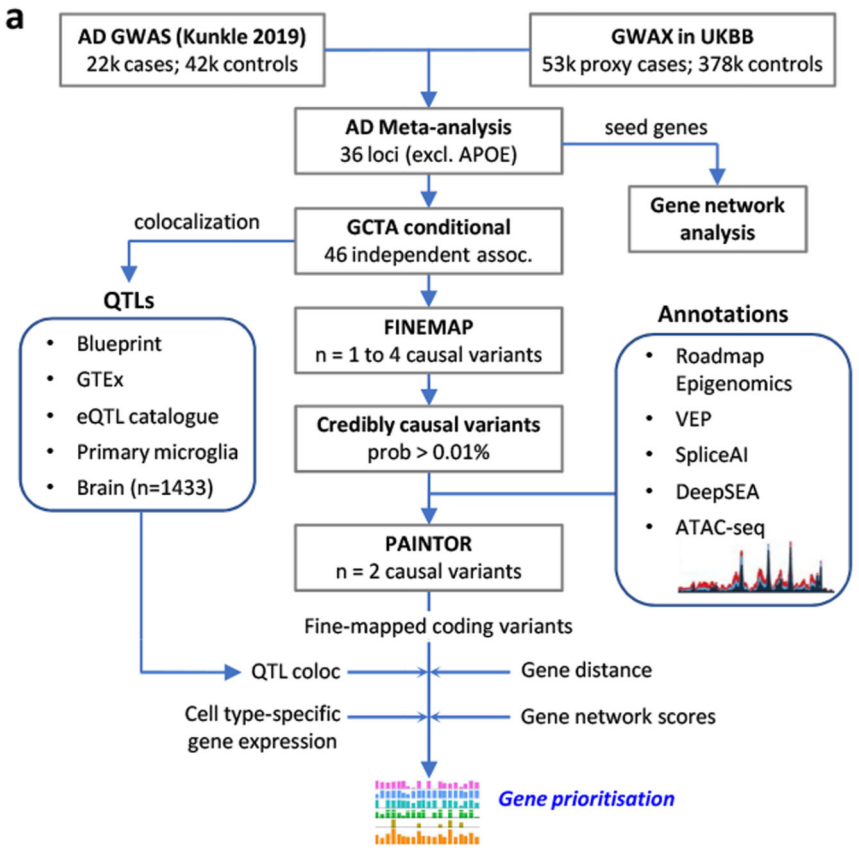

c	Locus	# signals	Lead p value
	APOE	see note	~0
	TREM2	3	1.83e-23
	BIN1	2	1.10e-54
	PTK2B-CLU	2	7.71e-26
	ABCA7	2	2.41e-13
	NCK2	2	1.28e-12
	EPHA1	2	9.63e-12
	ADAM10	2	2.67e-11
	ACE	2	1.21e-08
	APP-ADAMTS1	2	3.09e-08
	*PLCG2**	1	5.46e-08
	CLNK	1	2.59e-11
	SCIMP	1	1.35e-09
	SPPL2A	1	1.74e-09
	TSPAN14	1	2.74e-09
	VKORC1	1	4.47e-09
	APH1B	1	1.05e-08
	SPRED2	1	1.54e-08
	CCDC6	1	3.80e-08
	ADAMTS4	1	4.30e-08
	TMEM163	1	5.24e-08
	IKZF1	1	7.68e-08
	TSPOAP1	1	3.07e-07

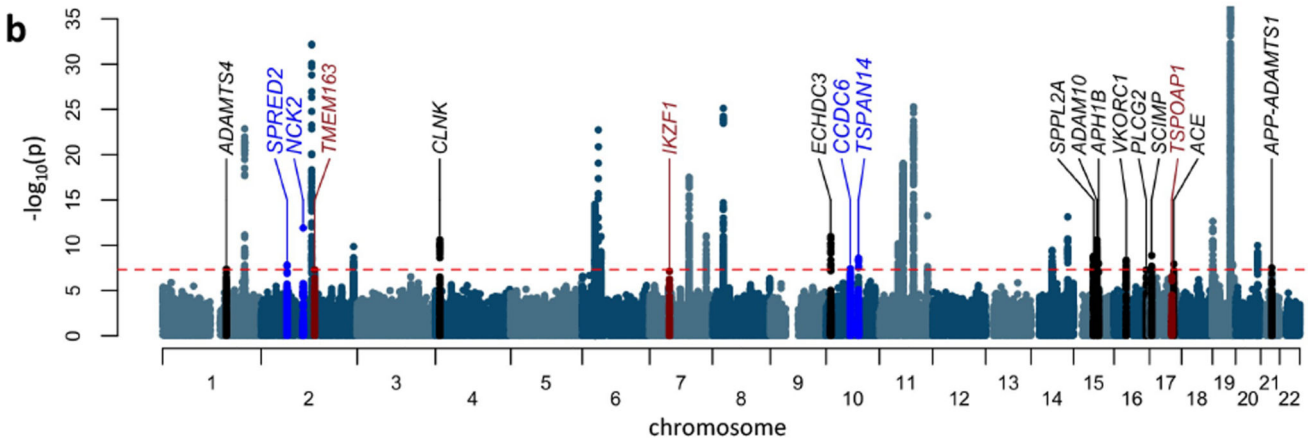

Figure 1. Analysis overview.

a, Summary of AD meta-analysis and data processing steps. **b**, Manhattan plot of the meta-analysis of GWAS for diagnosed AD and our GWAX in UK Biobank. Novel genome-wide significant loci are labelled in blue, sub-threshold loci in red, and recently discovered loci[2,3,12] replicated in our analysis in black. **c**, The number of independent signals at each locus which is either recently discovered or which has more than one signal, as well as the meta-analysis *P* value the lead SNP at the locus. *The *PLCG2* locus was significant ($P < 5 \times 10^{-8}$) when including Kunkle stage 3 SNPs. Conditional analyses were not done at *APOE* due to the strength of the signal (see Methods).

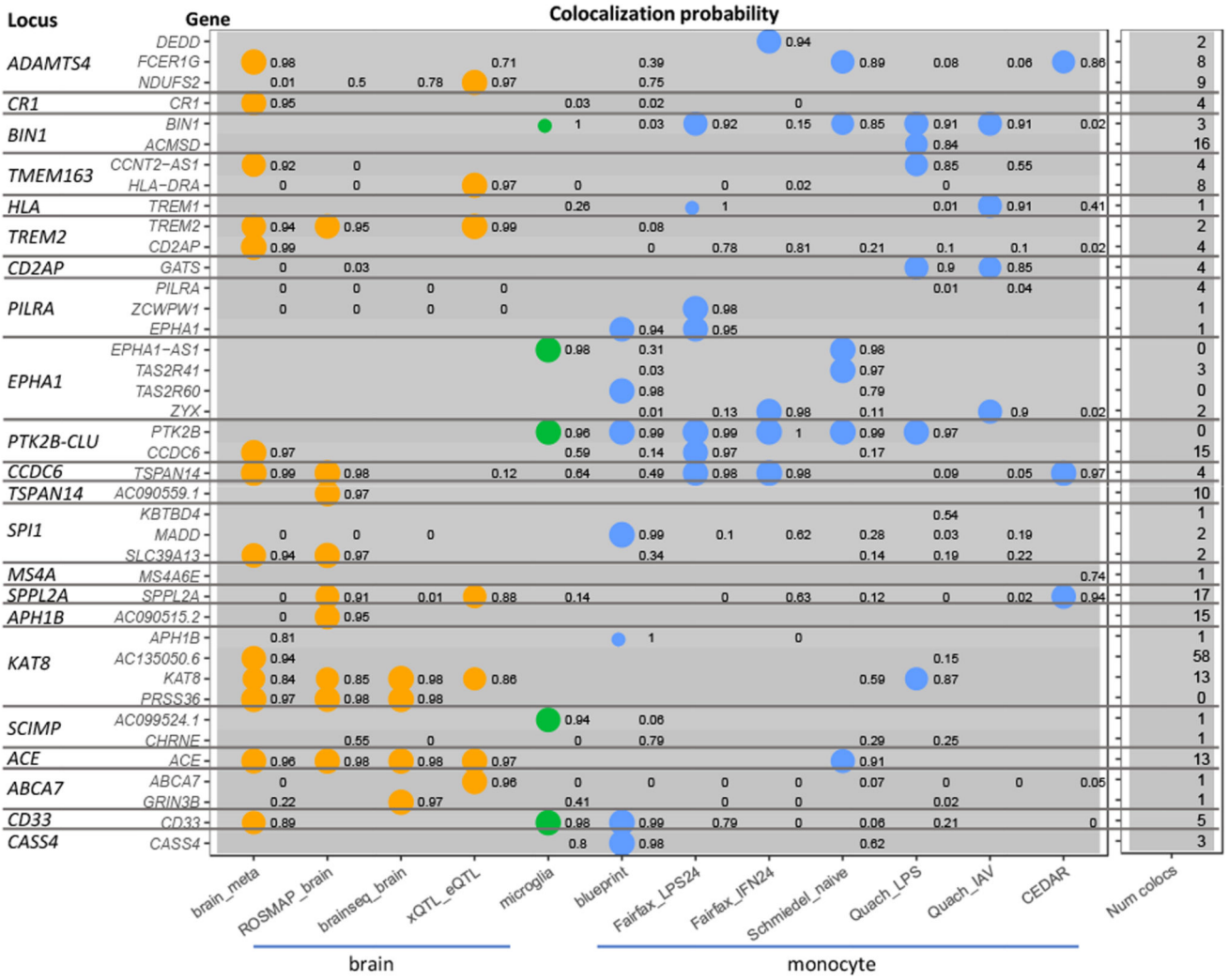

Figure 2. Colocalization with eQTLs.

For genes with the top overall colocalization scores across AD risk loci, the colocalization probability (H4) is shown for selected brain, microglia, and monocyte eQTL datasets. For three loci with multiple signals (*BIN1*, *EPHA1*, *PTK2B-CLU*), scores are shown separately for the conditionally independent signals. The last column shows, for each gene, the number of eQTL datasets with a colocalization probability above 0.8 (Supplementary Tables 5 and 6).

Europe PMC Funders Author Manuscripts

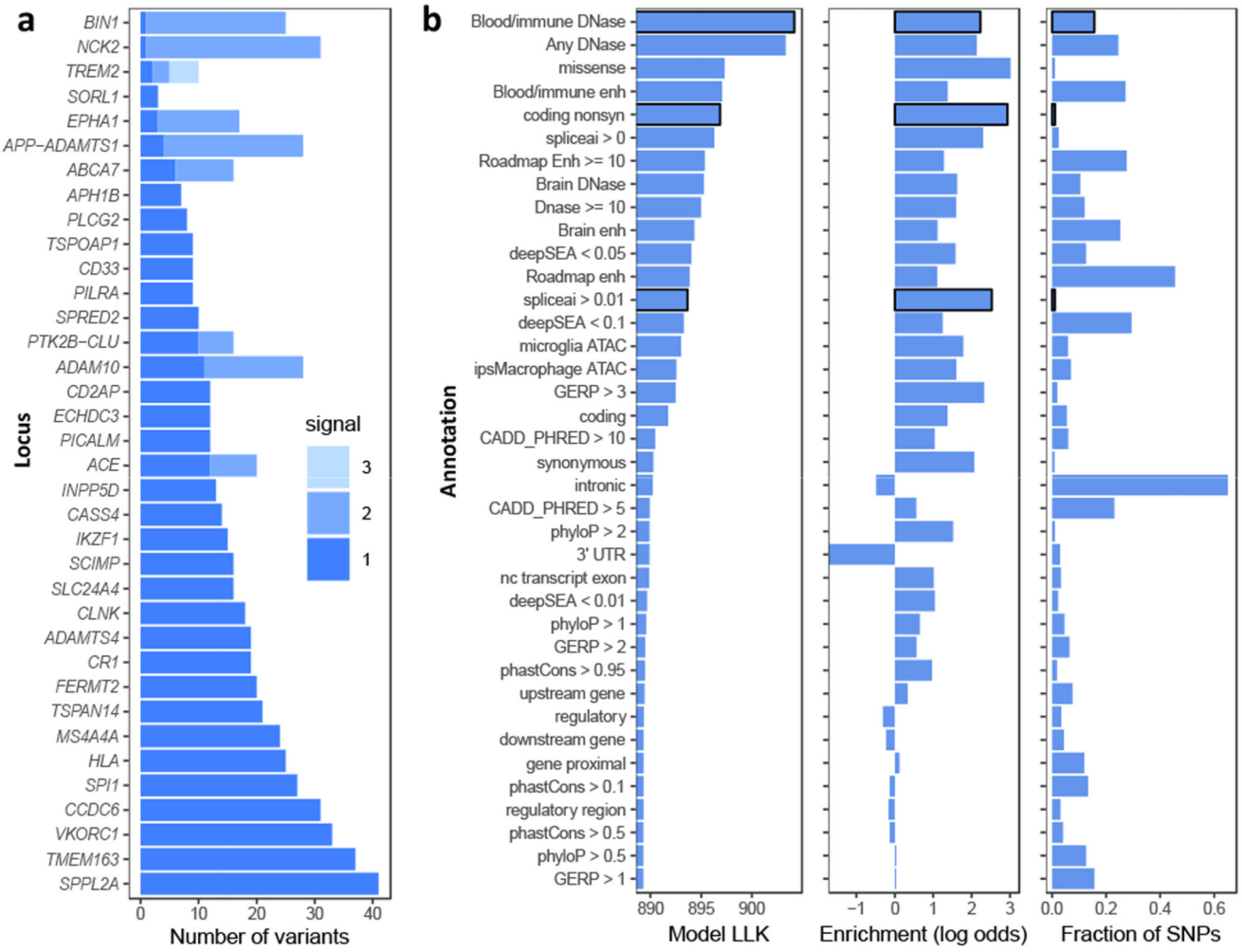

Figure 3. Fine-mapping summary.

a, Number of variants with mean causal probability > 1% for each independent signal. Variant counts for independent signals are shown in different shades. **b**, PAINTOR outputs, showing (left) log-likelihood (LLK) of model for each individual annotation; (middle) log-odds enrichments for individual genomic annotations determined by PAINTOR; (right) fraction of SNPs which are in each annotation (among those selected by FINEMAP probability > 0.01%). Annotations selected for the final model are shown with a black border.

Europe PMC Funders Author Manuscripts

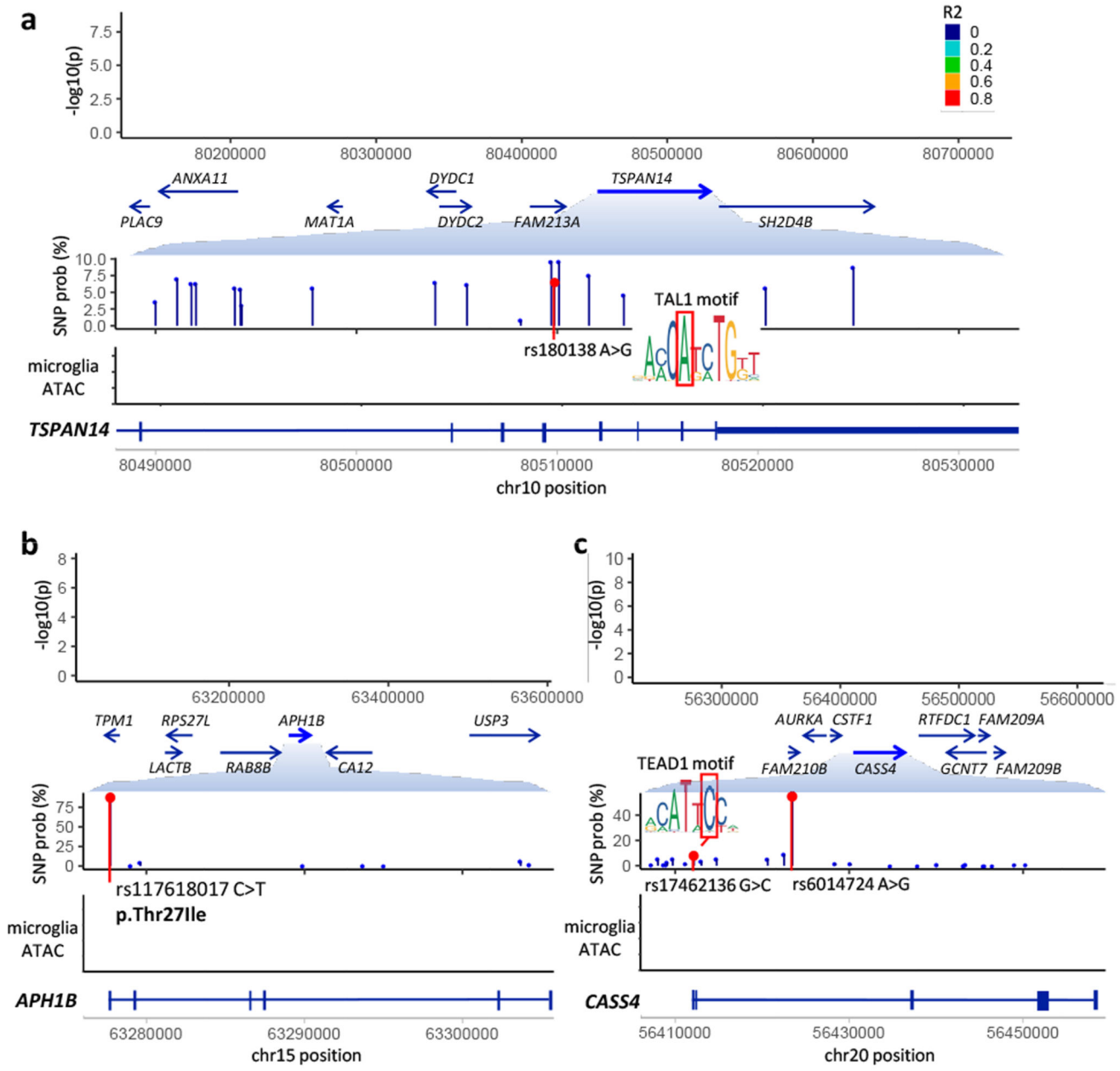

Figure 4. Fine-mapped variants.

a, SNP rs1870138 in an intron of *TSPAN14* disrupts an invariant position of a TAL1 motif. **b**, Missense SNP rs117618017 in exon 1 of *APH1B*. **c**, SNP rs17462136 in the 5' UTR of *CASS4* introduces a TEAD1 motif. Each panel shows (top) locus plot with GWAS *P*-values, SNP color representing LD to the lead SNP; (middle) expanded view of a subregion showing the mean SNP probabilities from fine-mapping; (bottom) read density of ATAC-sequencing assay from primary microglia[52].

Europe PMC Funders Author Manuscripts

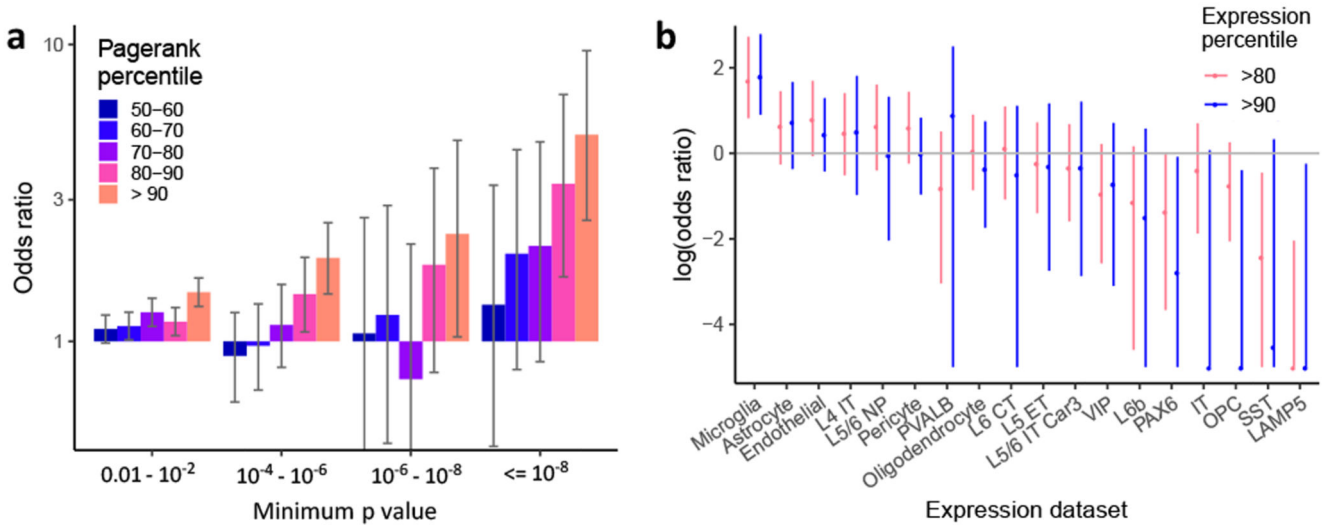

Figure 5. Genome-wide network and gene expression enrichments.

a, Enrichment of low GWAS *P* values within 10 kb of genes having high vs. low network pagerank percentile (low defined as below 50th percentile). Whiskers represent 95% confidence intervals based on Fisher's exact test for $n = 18{,}055$ genes. **b**, Enrichment of AD risk near genes with high expression in each brain cell type (above 80th or 90th percentile) relative to the other cell types. Cell types are defined based on single-cell clusters defined in Hodge et al.[77]. Neuronal cells are defined either by cortical layer (L4, L5, L6), and/or by projection target (IT, intratelencephalic; CT, corticothalamic; ET, extratelencephalic-pyramidal tract; NP, near-projecting), or by binary marker genes (LAMP5, PAX6, PVALB, VIP, SST). OPC, oligodendrocyte precursor cells. Whiskers represent 95% confidence intervals as determined by fgwas.

Europe PMC Funders Author Manuscripts

Europe PMC Funders Author Manuscripts

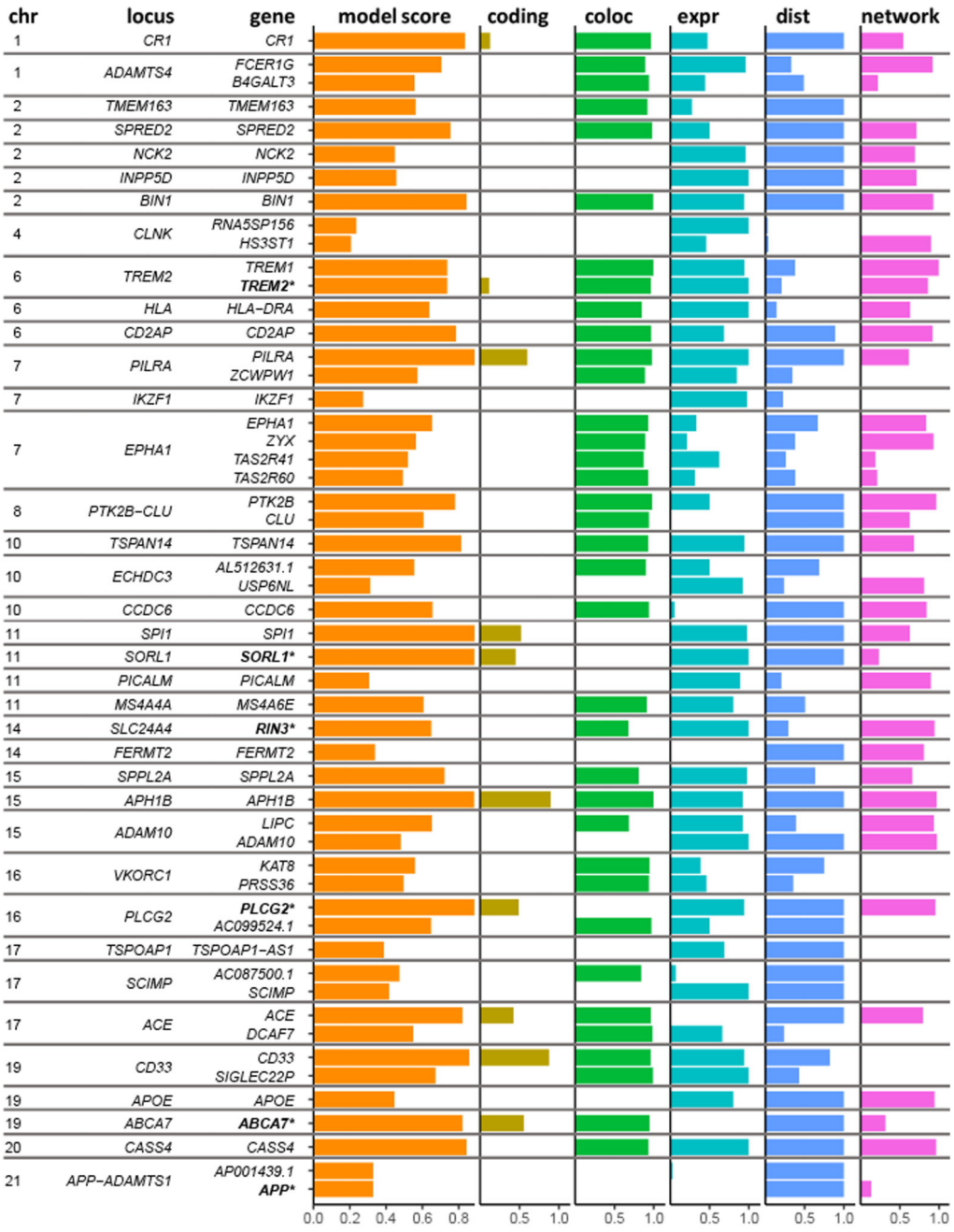

Figure 6. Gene evidence summary.

The top gene at each locus is shown, as well as the next 13 top genes by model score; for three loci where a non-coding gene was the top scoring, we also show the top scoring protein-coding gene. Score components for each gene are indicated by colored bars, and points show the distribution of scores for all genes within 500 kb at the locus. Bold gene names are those with evidence of causality based on rare variants from other studies. Scores for all genes are listed in Supplementary Table 13.

Europe PMC Funders Author Manuscripts

Table 1

Top candidate variants

Locus	SNP	*P* value	Odds ratio	Effect allele	Allele freq	SNP prob	SpliceAI	DeepSEA	Note	Refs
ADAMTS4	rs2070902	1.64E-06	0.949	T	0.2580	0.384	0.107	0.140	Intronic in candidate gene *FCER1G*, with predicted splicing change	
ADAMTS4	rs4575098	4.30E-08	1.063	A	0.2350	0.339		0.033	3' UTR of *ADAMTS4*, open chromatin	2
SPRED2	rs268120	2.08E-08	1.063	A	0.2502	0.556		0.033	Strong DNase peak, predicted by DeepSEA to decrease	
NCK2	rs143080277	1.28E-12	0.594	T	0.9957	1.000		0.086	Enhancer (Roadmap)	
BIN1	rs6733839	1.10E-54	1.168	T	0.3915	0.998		0.027	Microglia ATAC peak. DeepSEA predicts decreased DNaseHS	14,40
INPP5D	rs10933431	1.41E-10	1.080	C	0.7817	0.833		0.022		60
PILRA	rs1859788	3.28E-18	0.914	A	0.3206	0.601	0.008	0.041	Known PILRA missense G78R	41
ECHDC3	rs7920721	1.08E-11	0.935	A	0.6195	0.641		0.026	DNase peak. DeepSEA predicts changed binding of USF, Max, Myc	61,62
TSPAN14	rs1870137	2.93E-09	0.932	C	0.2056	0.097		0.007	Top DeepSEA variant, predicting decreased binding of HNF4, FOXA1, SP1	
TSPAN14	rs1870138	4.51E-09	0.933	A	0.2057	0.068		0.004	Highlighted in text; predicted loss of TAL1 binding	
SORL1	rs11218343	5.59E-14	1.205	T	0.9630	1.000		0.209		63
SORL1	rs2298813	1.52E-04	1.089	A	0.0470	0.451	0.054	0.003	Secondary association. Missense; also top DeepSEA variant	
APH1B	rs117618017	1.05E-08	1.089	T	0.1395	0.895	0.007	0.019	Highlighted in text; missense Thr27Ile	64
PLCG2	rs12444183	5.46E-08	0.948	A	0.3830	0.686		0.220	Near promoter of ncRNA AC099524.1, with strong microglia colocalization	2
PLCG2	rs72824905	6.35E-06	1.310	C	0.9924	0.492	0.018	0.006	Secondary association; known missense Pro522Arg. Top DeepSEA score	9
TSPOAP1	rs2632516	3.12E-07	0.952	C	0.4426	0.412		0.126	Overlaps ncRNA containing mir-142, important for hematopoietic development	62,65
TSPOAP1	rs2526377	8.45E-07	1.049	A	0.5579	0.169		0.006	Top DeepSEA variant (decreased DNaseHS) in microglial ATAC peak	66

Europe PMC Funders Author Manuscripts

Locus	SNP	*P* value	Odds ratio	Effect allele	Allele freq	SNP prob	SpliceAI	DeepSEA	Note	Refs
ACE	rs4311	1.21E-08	0.947	T	0.4704	0.490	0.126	0.053	Strong predicted splicing change	67,68
ACE	rs3730025	2.58E-07	0.819	A	0.9828	0.416	0.002	0.021	Secondary association; low-frequency missense Tyr244Cys	
ABCA7	rs12151021	2.41E-13	1.080	A	0.3258	0.713	0.013	0.312	Lead *ABCA7* variant	
ABCA7	rs4147918	7.63E-07	1.128	A	0.9587	0.552	0.071	0.045	Seondary association; missense Gln905Arg; predicted splicing change	69
CD33	rs12459419	2.02E-08	0.944	T	0.3256	0.662	0.001	0.070	Known missense Ala14Val; strong splicing QTL	7
CASS4	rs6014724	1.07E-10	1.116	A	0.9122	0.548		0.083	Lead *CASS4* variant	
CASS4	rs17462136	1.01E-09	0.901	C	0.0872	0.067		0.001	5’ UTR of *CASS4*; global top DeepSEA variant predicting decreased TF binding	
ADAMTS1	rs2830489	3.09E-08	0.943	T	0.2749	0.718		0.077	Lead variant near *ADAMTS1*	

A selected list of the most likely causal variants across loci, based on a combination SNP fine-mapping probabilities and annotations. Column ‘SNP prob’ indicates the mean fine-mapping probability for the SNP; the SpliceAI score is the maximum splicing probability for donor gain/loss or acceptor gain/loss, with nonzero values highly enriched for splicing effects; the DeepSEA functional significance score represents the significance above expectation for chromatin feature changes, as well as evolutionary conservation, with lower values more significant. References for specific SNPs are shown[2,7,9,14,42,43,61–70].